Antarctic geothermal heat flow and its implications for tectonics and ice sheets

Anya M. Reading[1,2]✉, *Tobias Stål*[1,2], *Jacqueline A. Halpin*[2,3], *Mareen Lösing*[4], *Jörg Ebbing*[4], *Weisen Shen*[5], *Felicity S. McCormack*[6], *Christine S. Siddoway*[7] *and Derrick Hasterok*[8]

Abstract | Geothermal heat flow (GHF) is an elusive physical property, yet it can reveal past and present plate tectonic processes. In Antarctica, GHF has further consequences in predicting the response of ice sheets to climate change. In this Review, we discuss variations in Antarctic GHF models based on geophysical methods and draw insights into tectonics and GHF model usage for ice sheet modelling. The inferred GHF at continental scale for West Antarctica (up to 119 mW m^{-2}, 95th percentile) points to numerous contributing influences, including non-steady state neotectonic processes. Combined influences cause especially high values in the vicinity of the Thwaites Glacier, a location critical for the accurate prediction of accelerated loss of Antarctic ice mass. The inferred variations across East Antarctica are more subtle (up to 66 mW m^{-2}, 95th percentile), where slightly elevated values in some locations correspond to the influence of thinned lithosphere and tectonic units with concentrations of heat-producing elements. Fine-scale anomalies owing to heat-producing elements and horizontal components of heat flow are important for regional modelling. GHF maps comprising central values with these fine-scale anomalies captured within uncertainty bounds can thus enable improved ensemble-based ice sheet model predictions of Antarctic ice loss.

Heat
Energy held by a substance owing to the vibration of molecules.

Geothermal heat flow (GHF)
The outward movement of heat, due to cooling and radioactive decay, through the Earth. Commonly reported as a value for near-surface layers in units of W m^{-2} or mW m^{-2}.

✉*e-mail: anya.reading@utas.edu.au*

https://doi.org/10.1038/s43017-022-00348-y

Heat from the hot interior of the Earth (FIG. 1) provides the energy that drives plate tectonic processes. The geothermal heat flow (GHF; expressed in mW m^{-2}; see BOX 1) measured at the Earth's surface is the sum of heat contributions from cooling and radiogenic heat production[1,2] within the Earth, and is highly variable across continental regions. Influences on GHF include lithospheric and crustal structure, tectonic setting, composition, neotectonics (that is, currently active plate tectonic processes including volcanism and anomalous mantle heat) and the presence of fluids (FIG. 1). Many aspects of tectonics can thereby be inferred from GHF. In the case of Antarctica, there is an urgent need for knowledge of subglacial characteristics such as GHF to provide input boundary conditions for predictive modelling of ice sheet change[3]. Further interdisciplinary applications of GHF anomaly maps include discerning suitable locations for oldest ice cores to reconstruct the Earth's past climate[4] and enabling insight into subglacial habitats[5] (FIG. 2).

The spatial distribution of continental GHF for Antarctica is potentially important for understanding past and present tectonic processes for this continent, given the extensive ice cover and limited rock exposure, provided that the multiple possible influences on GHF can be separated. However, factors such as shallow crustal heat production and refraction of GHF due to subglacial topography can cause local GHF anomalies (FIG. 1, BOX 1) that regional subsets of continental GHF maps cannot capture, owing to resolution limitations of constraining datasets. As GHF is an input boundary condition for ice sheet modelling[6], use of GHF maps without considering such local factors could pose a risk to the predictive capability of ice sheet models in some cases. Accurate prediction of accelerated ice loss in locations that could become tipping points (notably Thwaites Glacier of West Antarctica)[7] has potentially high consequences as these could become irreversible changes to part of the Earth's climate system[8].

GHF remains one of the least-known physical properties in global geoscience[9]. Constructing reliable, evenly distributed, global heat flow databases based on such in situ values[10,11] is difficult[12], and interpolation challenges are compounded by the differences between global GHF maps inferred using alternative geophysical techniques[13,14]. The high proportion of ice cover in Antarctica exacerbates these challenges due to high logistics costs and multiple open interpretations[15]. Additional maps, extracted from Antarctic GHF models that make use of empirical methods[16–18], are now

Key points

- Differences between geothermal heat flow maps for Antarctica that are derived using alternative approaches provide greater insight into its tectonic evolution than anomalies that are constrained from one model alone.
- Non-steady state processes and heat-producing elements in the upper crust contribute markedly to the spatial distribution of anomalously high geothermal heat flow values (>60%).
- High geothermal heat flow anomalies in West Antarctica are a consequence of multiple contributing sources, such as neotectonic rifting, volcanism and a mantle heat anomaly.
- The stable lithosphere of East Antarctica has relatively subtle geothermal heat flow anomalies, many of which are difficult to separate from model uncertainties and currently remain unresolved.
- Fine-scale geothermal heat flow variations can be accounted for, through low and high bounds to possible geothermal heat flow in the form of uncertainty maps, to provide robust inputs to predictive modelling of Antarctic ice sheet evolution.
- Geothermal heat flow is a boundary condition for modelling ice loss. In particular, the fast-changing Thwaites Glacier of West Antarctica, and the outlet glaciers of the Wilkes and Aurora Basins of East Antarctica, are locations of great concern.

Steady state
A system where heat flows while each point remains at a constant temperature.

Non-steady state
A system of heat flow where points in the system are changing temperature, also known as transient heat flow.

Heat producing elements (HPE)
Elements, such as uranium, thorium and potassium, that produce substantial heat through radioactive decay, often more concentrated in some upper-crustal lithologies.

available: enabling models and their differences to be quantitatively compared[19,20], exposing further insights into tectonic processes and with important implications for ice sheet modelling.

In this Review, we extend previous comparisons[15,21] and capture subsequent results including those based on independent multivariate empirical approaches[17,18,20]. We use the differences between mapped results together with their underlying inference methodologies and uncertainties to provide insights into the mechanisms that result in GHF anomalies in both West and East Antarctic lithosphere. Through interpretations of these GHF anomalies, we discuss the neotectonic processes and tectonic history for Antarctica. We outline best practice in making use of GHF maps in interdisciplinary research, for example as boundary conditions for modelling to inform the response of Antarctic ice sheets to global climate change.

Heat from the Earth

The core, mantle and crust provide a framework for considering the physical and chemical thermal processes of the planetary interior and the transfer of heat to the cooler exterior[22], which must reconcile with the observed total at the surface. Given the high uncertainty associated with the interior, heat in the deep Earth is considered in terms of a heat budget, whereby constraining one source places a bound on the balance[23]. In this section, we summarize the different contributors to GHF, measurements that enable GHF to be calculated, and key aspects of GHF as it interacts with the cryosphere.

Heat transfer to the surface

Theoretical estimates of the global magnitude of heat flux (unit W) from the deep Earth are highly uncertain, so the values that follow are provided to illustrate the relative sizes of the largest components of the Earth's internal heat budget. The heat flux outwards from the core (~10 TW) receives additions from the lower mantle (15–27, or ~23.5 TW); the upper mantle (~5 TW); and the crust (~7 TW), forming a total budget of ~45.5 TW (REF.[23]). The component due to radiogenic sources is estimated at ~19 TW (REFS.[24,25]) or ~42%, and the wide range for the lower mantle relates to the uncertain influence of convection in the upper mantle.

Heat transport through the lithosphere is predominantly by conduction (FIG. 1, BOX 1). In stable continental regions, the heat flow (heat flux density, unit W m^{-2}) is mostly steady state. In tectonically active regions, heat flow is transient, varying over time, and is hence in a non-steady state. Such transient processes are predominantly conductive[26], although advection can be important in the case of vertical fault movements, transport of magma, and high rates of sedimentation and erosion. At ocean ridges, advection brings melt to the surface, creating the crust that then cools by conduction. An average value of GHF across the Moho, consistent with the global budget, is 15 mW m^{-2} with lateral variation suggested to be limited owing to the small amount of radiogenic source material in the lithospheric mantle[2]. This value accords with the constraint that heat passing into the crust must be less than that measured at the surface to allow for the addition of a substantial radiogenic crustal component.

From an observational perspective, global maps have been constructed using grid-based approaches[10] consistent with a heat flux of 44–47 TW at the Earth's surface. A finer-resolution grid, made possible by assigning a GHF value to a geographical location with statistical support from multiple geological and geophysical observables[27], leads to an alternative determination[11] at 40–42 TW supporting a total value at the lower end of the range of currently accepted estimates of global heat budget. The mean GHF for the continents[11] is estimated at 67 mW m^{-2}, with the value for the oceans being higher, 79 mW m^{-2}, as younger oceanic plates cool, approaching a steady state lithosphere.

Heat sources in the crust

The radiogenic heat added by the crust (A, W m^{-3}) is provided by the decay of Heat producing elements (HPE) uranium, thorium and potassium, found in some lithologies typically concentrated in the Earth's continental upper crust[2]. Looking at granites[28,29], the heat production variation can mostly be explained by variations in the bulk composition, but there is also a relationship between heat production and crystallization age. Archaean crust, on average, adds 27 mW m^{-2} to the heat flow across the Moho to form the total of 42 mW m^{-2} for cratons of this age[30]. A more general analysis[31,32] finds an

Author addresses

[1]School of Natural Sciences (Physics), University of Tasmania, Hobart, Tasmania, Australia.
[2]The Australian Centre for Excellence in Antarctic Science, University of Tasmania, Hobart, Tasmania, Australia.
[3]Institute for Marine and Antarctic Studies, University of Tasmania, Hobart, Tasmania, Australia.
[4]Institute of Geosciences, Kiel University, Kiel, Germany.
[5]Department of Geosciences, Stony Brook University, Stony Brook, NY, USA.
[6]Securing Antarctica's Environmental Future, School of Earth, Atmosphere and Environment, Monash University, Clayton, Victoria, Australia.
[7]Department of Geology, Colorado College, Colorado Springs, CO, USA.
[8]Department of Earth Sciences, University of Adelaide, North Terrace, South Australia, Australia.

Temperature
A property of a material that defines the amount of heat energy available for transfer.

Cold-based
A cold-based ice sheet is an extensive body of ice where the base is below the pressure melting point.

Warm-based
A warm-based ice sheet is an extensive body of ice where the base is above the pressure melting point, and meltwater can be present.

increase in heat production of approximately fourfold from the Archaean into the Palaeoproterozoic (mostly independent of composition), and a relatively constant heat production from that time to the present.

Modelled GHF estimates generally add the crustal component to the mantle component by integrating the total heat production through the crust, the latter being dependent on the vertical distribution of heat-generating rocks. Observations from granulites formed at mid-to-lower crustal levels show that some heat production through most of the crustal column is plausible[30]. However, horizontal stratification with higher upper-crustal heat production[33–35] is found more generally. GHF anomalies, and hence individual values, are strongly dependent on length scale (even in stable tectonic regions), suggesting that most sources are located in the shallow part of the heterogenous upper crust.

GHF from direct measurements

GHF (q, W m^{-2}) can be calculated from direct measurements of temperature[9,36] in a borehole (FIG. 1, BOX 1), or using a probe in the case of soft sediments (common in offshore measurements), provided the thermal conductivity, k, can be determined or estimated. Such measurements enable a precise GHF value for the given location, but the context of the point measurement should be known[37,38]. Without such context, it is not evident whether the GHF value is representative of (say) a 20 km square polygon. Sampling bias towards regions of high heat flow is likely in the global catalogue[12].

Temperature measured in ice boreholes[39] or subglacial sediment[40,41] enables in situ determinations of GHF in Antarctica. Such locally obtained values are few, and for West Antarctica are characterized by their spatial variability, attributed to neotectonic or hydrothermal influences. Although it is tempting to use an in situ value of GHF as a constraint on regional GHF, such a value would be best obtained from a grid of measurements in the knowledge of high-resolution subsurface geology and thermal properties, that is, a highly demanding field campaign. Such subsurface information is of particular importance for ice sheet measurements[42] given that the thermal conductivity of ice falls in the intermediate range of possible rock values (BOX 1).

Geothermal heat and the cryosphere

GHF can be constrained through its effect on an overlying ice sheet in a number of ways[15], which are briefly summarized in this section. A numerical approach[43] has enabled an analysis of basal conditions for the Antarctic ice sheet, correlated using a seismic tomography result[13], and refined using glaciological observations. A key threshold point occurs when the basal temperature is equal to the pressure melting point (0 °C – 0.9H, where H is the ice thickness in km), which provides a constraint on the minimum likely GHF. It is estimated that 55% of the grounded ice of Antarctica is at the pressure melting point[43]. Perhaps counterintuitively, the outer 800 km of the East Antarctic Ice Sheet is cold-based, to first order, with the interior areas of the East Antarctic Ice Sheet being warm-based. In Antarctica, subglacial hydrology including subglacial groundwater is being increasingly considered[44,45] in view of the potential impact on several aspects of ice sheet basal conditions.

The presence of subglacial water can be inferred from observations of the relative bed echo strength of radar data together with consideration of subglacial hydrology. In the case of the Thwaites Glacier[46], such methods

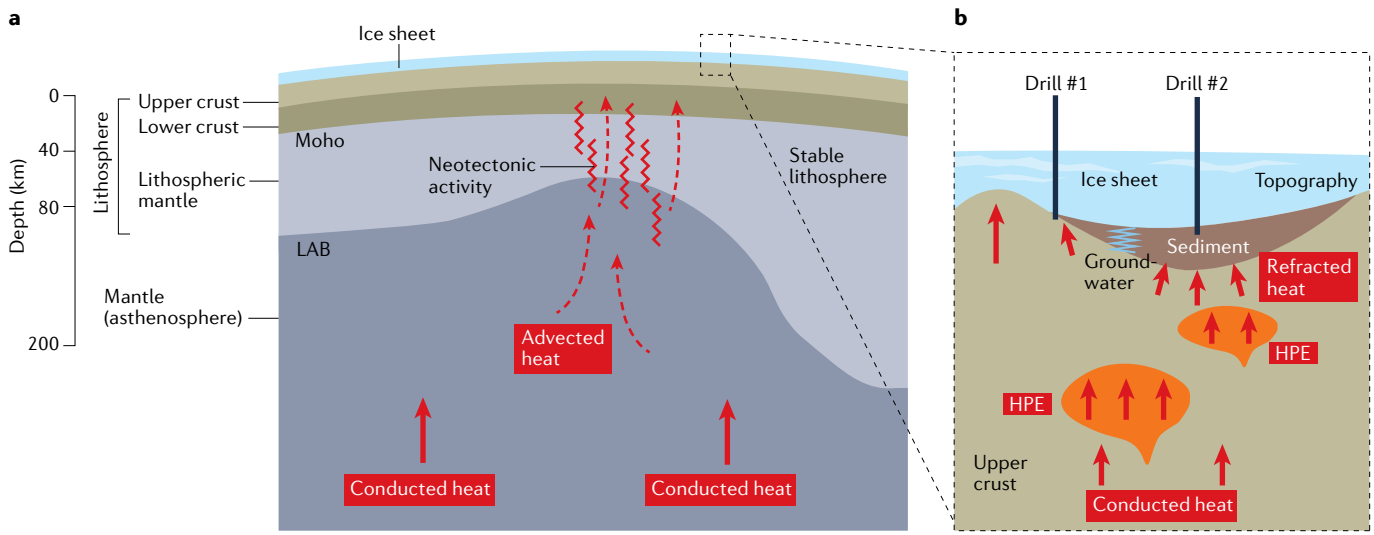

Fig. 1 | **Multiple contributors to geothermal heat flow. a** | Conducted heat from the deep Earth (straight red arrows), advected heat in the mantle (dashed curved arrows) and additional heat from heat-producing elements (HPE) such as igneous bodies in the crust all contribute to regional geothermal heat flow (GHF). **b** | More locally, features such as groundwater and refraction from subsurface layers can elevate or reduce regional GHF patterns. For example, Drill #1 provides a locally reduced GHF value due to the presence of groundwater, whereas Drill #2 provides a locally elevated GHF value due to the effects of a near-surface HPE and refraction due to subsurface geometry. Depending on local conditions, groundwater could also result in a locally enhanced GHF anomaly (such as near a hydrothermal heat source), and refraction could result in a locally reduced GHF anomaly. The depth scale is indicative: structural features and process can also occur at depths different from those shown. LAB, lithosphere–asthenosphere boundary. Heat sources from the deep Earth undergo additions and modifications by numerous influences, resulting in the spatial variability of the total GHF.

Box 1 | **Explaining heat flow**

Energy in the form of heat is transferred from higher-temperature inner layers of the Earth to cooler outer layers by conduction, whereby energy is exchanged between adjacent molecules[36]. Heat also moves through advection and mass transport, for example by deep and shallow hydrothermal groundwater fluids[180]; mantle convection driven by lower-density material rising and higher-density material sinking; and obduction, where material is forced upwards during tectonic plate collision.

Heat flow, q ($W\,m^{-2}$), between two layers of given area (see figure), in a given time, is proportional to the change in temperature, T, and inversely proportional to the change in depth, z. So

$$q = -k\frac{\Delta T}{\Delta z} + Az_{lith},$$

where the constant of proportionality is the thermal conductivity, k ($W\,m^{-1}K^{-1}$), which is usually measured as a laboratory sample or assumed on the basis of lithology[9]. Radiogenic heat production, A ($W\,m^{-3}$), is notable where a lithology of a given thickness z_{lith} includes heat-producing elements (HPE). These properties are integrated over a vertical column to find the total heat flow[36].

In the steady state case, heat flows through the system and each point in the system remains at a constant temperature. Steady state geothermal heat flow (GHF) comprises the heat flowing out from the lithosphere, plus the heat produced in the crust, most notably the upper crust.

In the non-steady state case (often termed transient), components of the system are changing temperature, usually cooling, indicating volcanic or other neotectonic activity. Owing to the long timescales of geothermal cooling in comparison to ice sheet processes, the term non-steady state is used in this Review.

GHF anomalies (red profiles in figure) occur due to rock units enriched in HPE[86], and through factors such as topography in the near-surface layers[42]. In the case of a shallow valley between sediment (Sed1) and ice, where $k_{Sed1} > k_{ice}$, a slight positive anomaly will result at the sediment–ice interface. Alternatively, for sediment (Sed2) where $k_{Sed2} < k_{ice}$, a slight negative anomaly will result. Typical values of k are: ice (>250 m deep) 2.15–2.75; igneous rocks 1.8–3.8; sedimentary rocks 1.5–5.6 $W\,m^{-1}K^{-1}$ (REF.[42]). The variations in k have a notable dependence on temperature[36].

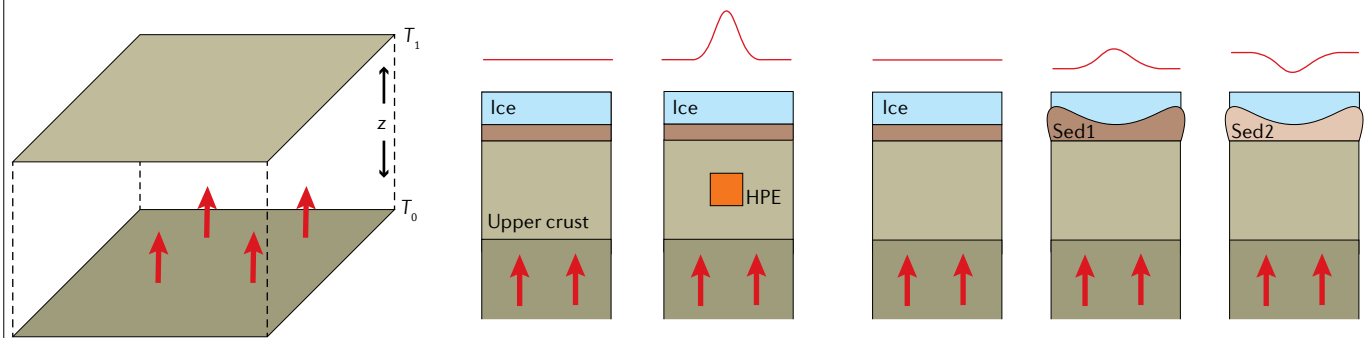

show elevated values and high spatial variability. The development of internal structure of ice sheets can be determined by using radar data to identify englacial stratigraphy and structures indicating enhanced basal melting[47]. A further observable that can be used to infer englacial temperature is microwave emissivity[48]. The presence or absence of larger bodies of liquid water in the form of subglacial lakes[49] is again usually inferred through airborne geophysical data or remote sensing approaches[50,51]. The absence of basal water, where the ice sheet is frozen to the bed, constrains the maximum GHF[52]. As noted previously[15], minimum and maximum constraints on GHF from glaciological approaches provide stronger lines of evidence for ice sheet basal conditions when used in combination.

Heat from cooling and radioactive processes from deep within the Earth flow outwards and combine with important additions from heat sources in the upper mantle and crust to form the total GHF. Values of GHF show high spatial variability and can be determined from in situ measurements or constrained by its effect on an overlying ice sheet. Models of GHF can also be determined by indirect means, making use of geophysical approaches.

GHF models of Antarctica

All GHF models determined using geophysical approaches show a clear contrast in the character of the mapped GHF between the physiographic provinces of West Antarctica (WA) and East Antarctica (EA). In this section, aspects of selected models for Antarctica (FIG. 2) are outlined in the context of its tectonic structure[53–55]. Model differences that can be directly linked to the approach used, and any underlying assumptions inherent in the approach, are also outlined. We make use of open-source data sharing initiatives for Antarctic geology, geochemistry and geochronology[56,57], which enable increasing consistency in the description of lithologies, compositions and ages.

Tectonic framework

Present-day WA is made up of distinct contrasting provinces, records magmatic events throughout the Phanerozoic[54], and shows extensive evidence for neotectonic activity[58] and internal deformation[59]. Assembled along the convergent southern margin of Gondwana, this extensive orogen (from what is now Australia to South America) has the complex West Antarctic Continental margin system[54] as its central portion. This complex system includes the continental terranes of Thurston Island, the extended, uplifted, Marie Byrd Land[60], and the well-exposed and well-preserved magmatic arc of the Antarctic Peninsula[54,61]. The crust between the exposed blocks is most usually interpreted as continental, more greatly extended and thinned in nature, with extension in the Weddell Sea sector in the Jurassic, and extension across Marie Byrd Land and Ross Embayment from the Cretaceous to the present, forming the West

Antarctic rift that holds the West Antarctic Ice Sheet. Geological elements of back-arc extension associated with oceanic subduction have also been discovered[54], and geophysics-based work extends this interpretation more broadly[62].

In contrast, continental EA has been largely stable since the end of the Ross Orogeny (500 Ma)[63] and is mostly concealed beneath the East Antarctic Ice Sheet, extensive areas of ice being 3,000–4,000 m thick. Consistent rotational motion across the whole of the EA continental block[64] suggests a very coherent lithosphere. Notable physiographical features have been identified using airborne geophysics: the Gamburtsev Subglacial Mountains rise to within 400 m of the ice surface[65,66], and the extensive Aurora and Wilkes Subglacial Basins lie mostly below sea level[67]. EA comprises cratonic blocks, notably the Mawson, Napier and Grunehogna, separated by wide mobile belts including *c*.1.3–0.9 Ga ('Grenvillian') orogens of substantial lateral extent and *c*. 0.65–0.5 Ga ('Pan-African') orogens with reworking of older orogens and further substantial additions[55]. The continental margins conjugate to Australia, India and South Africa resulted from the break-up of Gondwana during the Mesozoic–Cenozoic[63]. Crustal domains and boundaries have been identified through geological[63,68] and geophysical work[69,70] and plate tectonic reconstructions[71].

Spatial variation of GHF in Antarctica

The variation of GHF has been determined indirectly using empirical, forward modelling and combined approaches (TABLE 1, FIG. 2, Supplementary Note 1, Supplementary Fig. 1). Maps of the GHF of Antarctica all show higher values for WA than EA, as might be expected from the tectonic framework (FIG. 2): values for WA fall in the 59–119 mW m^{-2} range while those for EA are 45–66 mW m^{-2} (5th and 95th percentiles)[17]. The highest values of GHF occur inboard of the Amundsen Province of Marie Byrd Land[54], beneath the inland part of the Thwaites Glacier, in both empirical multivariate models[17,18]. A similar result has been obtained based on detailed geomagnetic surveys[72] although the highest part of the modelled anomaly falls on the Marie Byrd Land side of the Thwaites Glacier.

Notable model differences

We now review the most notable model differences (FIG. 2), noting that GHF for Antarctica must be indirectly inferred or calculated across large regions. In general, authors of the models are careful to outline their methods and underlying assumptions (Supplementary Note 2, Supplementary Fig. 2), so all models have contributed to progress in the field.

Maps based on multivariate empirical methodologies (FIG. 2a–c) incorporate the majority of available information[19] in constraining the spatial variation of GHF and have the advantage of clearly quantified uncertainty being part of the inference process (FIGS. 3 and 4, Supplementary Note 3, Supplementary Fig. 3). Such GHF maps are developed using statistical means; through the similarity approach[11,27], refined as in Aq1[17], or machine learning as in LE21[18]. Alternatively, the constraint methodology can make use of a single property such as seismic wave speed. Using such an empirical approach based on a seismic tomography result[73], with constraints based on a US database, yields a GHF map (SW20, FIG. 2c)[16] with elevated features in common with Aq1 and LE21. The US reference database has advantages in terms of its quality and detail for many locations, but some plausible tectonic settings are not captured (such as a rift-type environment). GHF mapped using a seismic tomography result, (SR04, FIG. 2d)[13], using a low-resolution global reference database including Antarctica, shows elevated values in the vicinity of the Byrd Subglacial Basin. Aq1 and LE21 also show elevated GHF values in this vicinity, with the high values extending across the Byrd Subglacial Basin to the Haag and Ellsworth blocks of the Weddell Sea sector. Aq1 shows generally higher values than LE21 through the West Antarctic rift to the inner Ross Ice Shelf. Aq1 and SW20 (TABLE 1) are subject to biases in the reference datasets (global and US, respectively), while machine learning approaches such as LE21 have some sensitivity to choices relating to individual input datasets.

Forward model-based approaches to calculating surface GHF depend on estimates of the geothermal gradient (geotherm), the variation of temperature with depth. Such approaches can make use of magnetic data to calculate depth to the Curie point isotherm (MC17[74] and FM05[75], FIG. 2e,f), or seismic data (AW15[76]) to calculate depth and temperature in the upper mantle, and have been used in interdisciplinary research[77]. Differences between forward models have been noted previously[15], and the apparent contradictions can be understood in terms of the constraint used[78,79] and the assumptions also inherent (TABLE 1, Supplementary Note 2). Magnetic-derived estimates can provide constraints within a single province[72], where the spatial variability in the impact of assumptions regarding the crustal contribution is less dominant.

3D models of seismic velocity inferred using seismic tomography provide a well-founded basis for constraining GHF models due to temperature being the most substantial control on mantle seismic velocities. Seismic results have been used to constrain the empirical approaches noted above[13,16], and also the lithospheric geotherm[76,80]. S-wave velocity is related, over an appropriate range of pressure and temperature, to elastic parameters and density with an anelastic correction[81,82]. The inferred values are capped at 90 mW m^{-2} owing to the theoretical limit on the thermal gradient for a steady state thermal model for the lithosphere[2]. In general, the seismic tomography model used to constrain the thermal structure of the lithosphere has an impact on subsequently calculated results[83,84]. In quantifying the incompatibility of some GHF models[85], the importance of accurately estimating the crustal contribution is demonstrated. When examined in detail[20], some locations in maps based on forward models[74–76] taken in isolation imply unrealistic thermal gradients at depth.

In summary, empirical results (Aq1, LE21, SW20 and SR04), forward modelling approaches (MC17 and FM05) and other approaches (Supplementary Fig. 1) capture the high values of GHF for WA, while the variation of

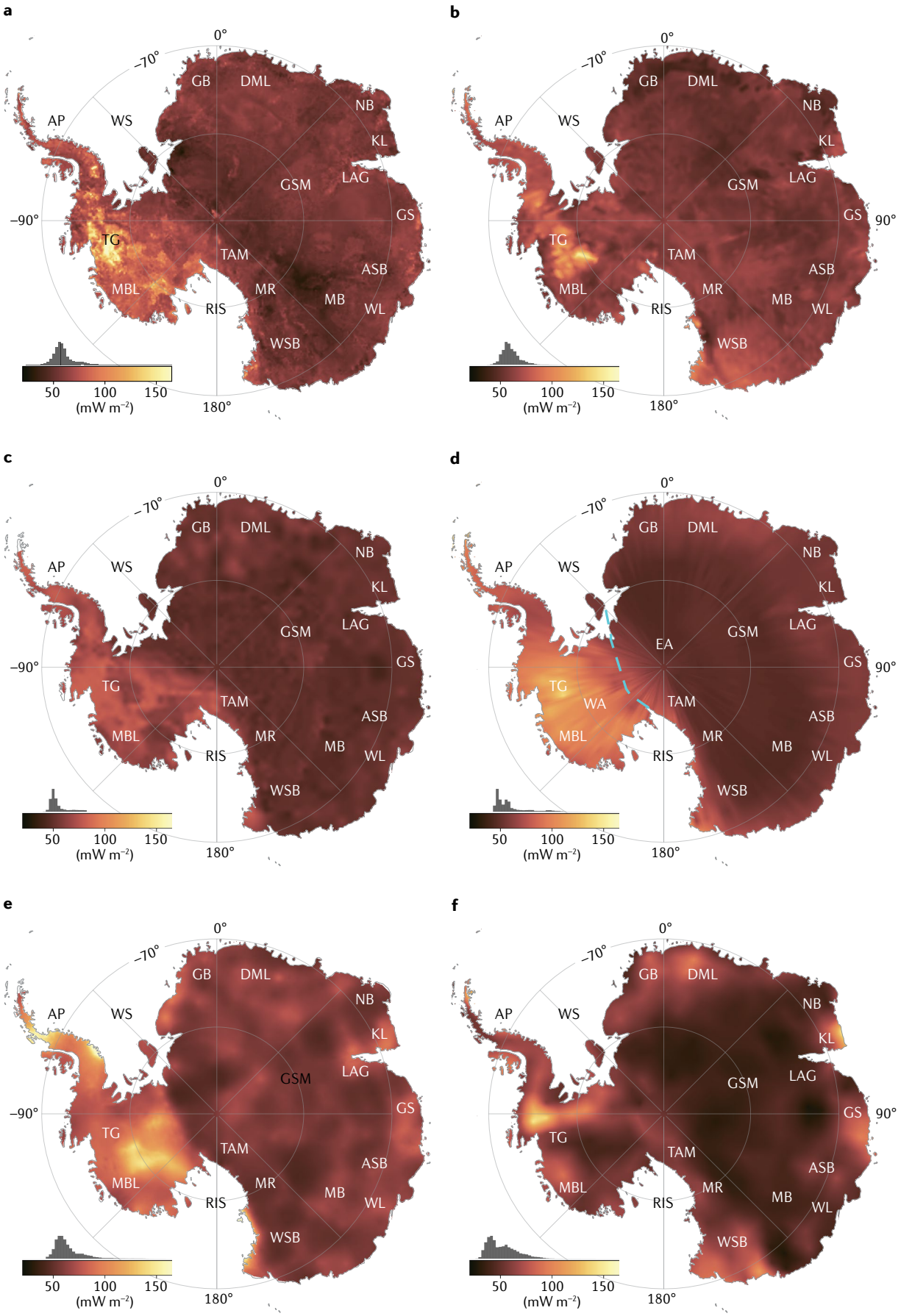
a
b
c
d
e
f
0°
−70°
−90°
90°
180°
AP
WS
GB
DML
NB
KL
LAG
GSM
GS
TG
TAM
ASB
MBL
MR
MB
WL
RIS
WSB
EA
WA
50
100
150
(mW m⁻²)

Fig. 2 | **GHF models of Antarctica.** Selected GHF models replotted using agrid[19,20] using colourmaps from REFS.[176,177] and clipped to the coastline or grounding line, with ranges displayed in the bottom left of each panel. **a** | Aq1[17] multivariate empirical model from statistical similarity[17]. **b** | LE21 (REF.[18]) multivariate empirical model from machine learning. **c** | SW20[16] empirical model from seismic tomography. **d** | SR04[13] empirical model from global seismic tomography. **e** | MC17 (REF.[74]) forward model from spectral analysis of magnetic data. **f** | FM05[75] forward model from equivalent dipole magnetic approach. Further models that have available data are provided in Supplementary Fig. 1 for comparison. The broad geographic division[178] between West Antarctica (WA) and East Antarctica (EA) is shown by the cyan dashed line in panel **d**. AP, Antarctic Peninsula; ASB, Aurora Subglacial Basin; DML, Dronning Maud Land; GB, Grunehogna block; GS, Gaussberg; GSM, Gamburtsev Subglacial Mountains; KL, Kemp Land; LAG, Lambert–Amery Glacier; MB, Mawson block; MBL, Marie Byrd Land; MR, Miller Range; NB, Napier block; RIS, Ross Ice Shelf; RP, Ross Province; TAM, Transantarctic Mountains; TG, Thwaites Glacier; WL, Wilkes Land; WS, Weddell Sea; WSB, Wilkes Subglacial Basin. GHF models of Antarctica show agreement in their broad-scale features, but considerable differences in the exact locations and shapes of high and low GHF anomalies. Panel **a** adapted with permission from REF.[17], Wiley.

the form of a given anomaly can be explained by one or more of the following: differences in model resolution, biases in reference datasets, sensitivity to input dataset choices, geotherm assignment or choice of crustal model component. Both seismic and magnetic data are used as input to the multivariate empirical maps (TABLE 1; Aq1 and LE21), providing a robust statistical combination of the constraints that they provide (Supplementary Note 2). Maps based on the average of values calculated using different approaches should be avoided in favour of research products where uncertainties are systematically quantified on a consistent statistical or physical basis (for example, using ensemble variance).

Geological constraints

Global appraisals of heat production values for different lithologies suggest how the crustal contribution is likely to affect estimates of the temperature of the lithosphere[86]. Analysis of transported rocks found in moraines provides clues to the subglacial lithologies of the EA interior[87]. The probable source area for such erratics is inferred using glacier flow lines, providing a geologically realistic sample set from which to infer the likely crustal contribution, and hence GHF. Further insights can be gained through modelling glacial detritus pathways given alternative ice sheet states[88].

Owing to the lack of geological exposure in the Antarctic interior, continental-scale forward models of GHF do not incorporate a crustal HPE contribution on the basis of observed geology; instead, an average value is assigned. Multivariate empirical models[17,18] include some geology-related observations, including the presence of volcanoes[89], and categorical tectonic regions[90], the latter reflecting likely crustal contributions to GHF but at a low resolution (Supplementary Note 2). Where there is exposed rock in Antarctica, it is possible to model the crustal contribution based on the abundance of HPE in field samples from geochemical analyses. An elevated regional-scale GHF, 80– 100 mW m^{-2}, is estimated for the Antarctic Peninsula[77] based on sample geochemistry added to the contribution from the deeper lithosphere constrained using seismology[76], noting the possibility of sampling bias.

If a heat-producing lithology is present in the uppermost crust, then values of 120 mW m^{-2} would not be exceptional. Such high values are consistent with a field-based approach[91] from East Antarctica that uses HPE abundances from exposed Cambrian granites to model GHF along a 270-km transect, showing several peaks above 80 mW m^{-2} and one peak above 120 mW m^{-2}. This approach allows detail in the form of high-GHF anomalies to be inferred, and indicates the likely scale length of anomalies. For a given location, it is important to note whether short-wavelength anomalies for the crust should be superposed on the long-wavelength anomaly, or whether the short- wavelength detail effectively sits within the long-wavelength envelope (FIG. 5).

Geological processes can affect the thermal structure of the crust and upper lithosphere if warmer material from lower down the steady state geotherm is raised to a shallower depth. In this situation, the shallow thermal structure would remain in a non-steady state for an extended interval of geological time[92]. Likewise, processes that mechanically lower the geotherm through depositional loading also result in a non-steady state thermal structure of the crust and uppermost mantle with artificially low temperatures for the given depth. Added sedimentary basin layers can show higher or lower heat production, and thermal conductivity, than the crystalline basement rocks.

Additional constraints and processes

Additional lines of research can be incorporated to improve the constraints placed on GHF. For example, approximations in the crustal contribution affect the values obtained for geotherms[33] into the deeper mantle. Temperature is the main factor to control seismic wave speed in the upper mantle[81,93]. For East Antarctica, temperature alone is insufficient to explain the gravity and topography variations, and some composition-controlled density variation is likely[83,94,95]. Seismic data are used to constrain the geochemistry of crust in other parts of the world including placing indirect constraints on the probable influence of HPE[96,97]. Investigations linked to viscosity variations[98] provide a further, indirect constraint on thermal structure, noting that glacial isostatic unloading and other factors could affect uplift rates and hence thermal property estimates. Thermal isostasy has been used as a basis for separating influences on GHF for the Australian continent[99], again revealing the impact of crustal contribution, and also the potential for sublithospheric heat flow. These approaches for Antarctica[100] have notable challenges owing to input data limitations, including the subglacial topography and other constraints, although the Australian case provides a further illustration of the potential to extract insights from GHF observations.

Conduction-based GHF models neglect the impact of other forms of heat transfer or generation, and the possible contribution of other processes affecting the inferred GHF should be considered. Mechanical processes such as ice-age cycling, which repeatedly changes lithospheric loading and aids the upward movement of small pockets of magma in the form of vug waves, have been invoked as a means of enhancing volcanism and GHF[101]. Hydrothermal transfer of heat in the shallow crust can have major impact on GHF estimates. Groundwater, for

example, can moderate local high-GHF anomalies and result in a faster attainment of a steady state condition[102]. Hydrothermal transfer of neotectonic, non-steady state heat can also lead to locally high in situ values for GHF. Such activity is noted as a source of bias in reference databases[11].

Models of GHF determined using different geophysical approaches can show differences related to the approach that is used. Such differences can be used to further explore the likely contributions to GHF anomalies.

Implications of GHF for tectonics

Using different methods to infer the spatial distribution of GHF in Antarctica enables the likely influences on GHF properties to be explored (FIGS. 3 and 4). The uncertainties in geophysical models[20,103,104] must be considered (Supplementary Note 3) as an inherent part of their interpretation. For example, when two models are compared at a given point on a map, the difference between them might not be significant when compared with the range of possible values that the model could take at that point. To explore some of the many influences on Antarctic GHF properties alongside their uncertainties, two models are compared alongside minimum and maximum difference maps (FIGS. 3 and 4). The influences at a given location add to form the resultant GHF (FIG. 1), noting that the different spatial scale lengths are a clue to multiple influences being active at that particular location (FIG. 5).

West Antarctica

Regions with active neotectonic processes in WA are identified by the elevated positive residuals when a steady state GHF model is subtracted from an empirical GHF model, as in the difference map Aq1[17] – AqSS[20] (FIG. 3b). In this case, the steady state components are the lithospheric mantle value with an added, simplified crustal contribution from HPE[105]. The remaining contributions could include non-steady state components such as neotectonic and hydrothermal influences, and also localized patches of high HPE abundance in the crust.

Neotectonics from non-steady state GHF. The broad region of the WA rift system[54,106] (spanning Marie Byrd Land and Ross Embayment) manifests in the spatial pattern of GHF as three subregions with elevated heat flow.

Table 1 | **Comparison of Antarctic GHF models**

Data type	Approach (identifier)	Description	Tectonic settings	Comparative resolution	Strengths	Cautions
Empirical modelling						
Multivariate	Statistical similarity, refined (Aq1)[17]	Multiple datasets link global geothermal heat flow (GHF) values to Antarctica	Broad range	Moderate[a] (variable)	Robust to the choice of input datasets	Relatively high uncertainty (Supplementary Note 3)
	Machine learning (LE21)[18]	Multiple datasets link global GHF values to Antarctica	Broad range	Moderate	Intermediate uncertainty	Some sensitivity to the choice of input datasets
Seismic tomography	Statistical similarity (SW20)[16]	Links GHF values from continental USA to Antarctica	Restricted range	Low[b] to moderate	Reference data and target are good quality and directly comparable	Some tectonic settings are not present in reference dataset
	Statistical similarity (SR04)[13]	Links GHF values from a global catalogue to Antarctica	Broad range	Very low[c]	Reference data and target are the same and target are the same	–
Forward modelling						
Seismic tomography	Seismic velocity (AW15)[76]	Constrains the upper-mantle geotherm	N/A	Low	Robust association between seismic velocity and temperature	Crustal thermal properties are assumed to be constant
Magnetic	Spectral analysis (MC17)[74]	Estimates the Curie temperature depth (CTD) isotherm	N/A	Moderate (variable)	–	(1) GHF does not always correlate with CTD. (2) Impact of averaged crustal component
	Equivalent dipole (FM05)[75,175]	Estimates the CTD isotherm	N/A	Low	Crustal component based on comparisons with other continents	–
Other						
Multivariate	Heat proxies (GV20)[174]	Estimates basal temperatures from direct observations	Broad range	Local values	–	–
Multivariate	Heat balance for stable lithosphere (AqSS)[20]	Estimates subcrustal component, crustal component from tectonic segmentation	Restricted range, excludes neotectonic settings by design	Low	No impact of assumptions relating to temperature in the upper mantle or lower crust	(1) Tectonic segment poorly constrained. (2) Reference model (steady state only)

[a]Moderate: 20–100 km. [b]Low: 100–400 km. [c]Very low: >400 km.

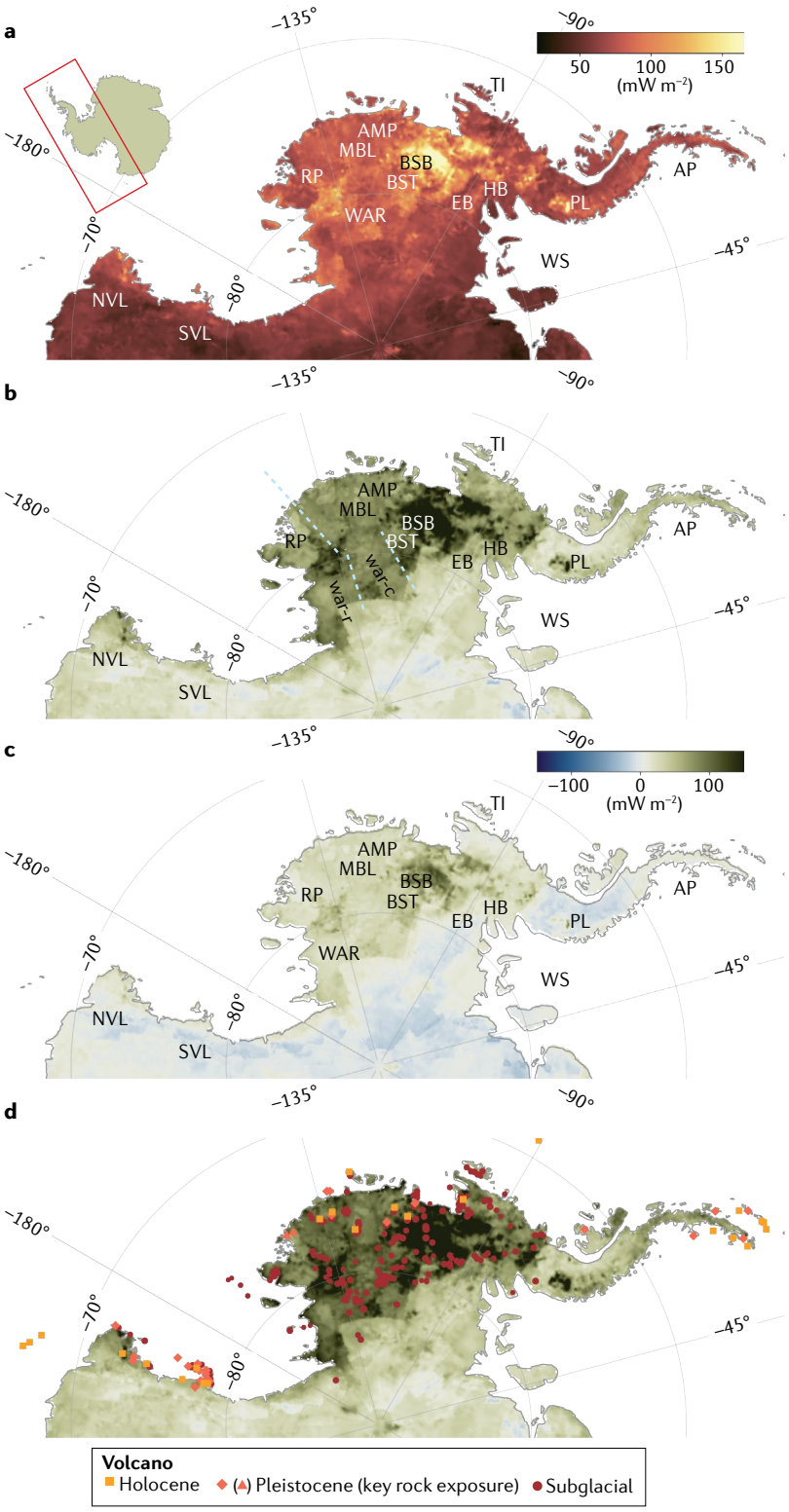

Fig. 3 | **West Antarctic GHF, and non-steady state and anomalous components. a** | Multivariate empirical model from statistical similarity, Aq1, as shown in FIG. 2a. **b** | Difference between Aq1[17] and a calculated steady state model, AqSS[20] (Aq1 – AqSS). The nominal geographic subregions discussed in the text are shown by cyan dashed lines, including war-c, West Antarctic rift-central, and war-r, West Antarctic rift-Ross. **c**,**d** | Panels **c** and **d** are companion plots to allow consideration of uncertainties: **c**, smallest absolute difference between allowed values of Aq1 and AqSS models; and **d**, largest absolute difference between allowed values of models, overlain by volcanoes and selected examples of Pleistocene volcanic rocks[109,122,179]. AMP, Amundsen Province; AP, Antarctic Peninsula; BSB, Byrd Subglacial Basin; BST, Bentley Subglacial Trench; EB, Ellsworth block; GL, Graham Land; HB, Haag block; MBL, Marie Byrd Land; NVL, Northern Victoria Land; PL, Palmer Land; RP, Ross Province; SVL, Southern Victoria Land; TI, Thurston Island; WAR, West Antarctic rift; WS, Weddell Sea. AqSS is produced in low resolution (Supplementary Fig. 1g) and inherits a step-like distribution in some locations from the categorical datasets[20], so although some sharp boundaries might be real, others could be artificially emphasized, and it is best to avoid any interpretations based solely on such features. Differences between models can reveal non-steady state and anomalous contributions to GHF.

The highest anomaly occurs between the Amundsen Province and the Ellsworth block, includes the Byrd Subglacial Basin (FIG. 3b: BSB), and implies neotectonic rift-related activity that exposes a source of GHF in non-steady state, potentially akin to either extended continental or oceanic crust[62,107] as a substantial contributor to the anomaly. This region, the focus of considerable attention due to observations of the rapid ocean-driven change of the Thwaites Glacier[108], is also characterized by thin crust and lithosphere, shallow Curie depths and high uplift rates[72]. Subglacial volcanoes have been proposed in this region and across much of the WA rift system and surrounding lithospheric blocks[109] (FIG. 3d), with the caveat that the underpinning datasets are non-uniform and interpretations are subject to revision as constraints improve.

The middle subregion (FIG. 3b: war-c) shows only moderately elevated difference values, similar to the Marie Byrd Land block, and hence appears to be closer to steady state than the other regions of the WA rift system. It is likely this region comprises moderately extended continental crust, hosting basins that hold subglacial sediments[110,111] upon deeper magnetic basement. Suggested subglacial volcanoes[109] cut across the boundary between the contrasting Byrd Subglacial Basin and WA rift-central subregions (FIG. 3b,d: BSB and war-c), suggesting an additional, younger, influence on the tectonic evolution, although there is no addition to the present-day GHF inferred for this subregion.

The Ross subregion of the WA rift (FIG. 3b, war-r) shows elevated difference values. The WA rift system in this subregion has been identified as highly extended continental crust[112,113] with a limit corresponding to the boundary between subregions (FIG. 3b, war-r and war-c). The strongest trend line in the suggested subglacial volcanoes[109] appears not to cross the boundary in this case. This region is of ongoing interest given the probable interplay between ice sheet evolution and the subglacial geology[110]. It features active normal faults and displays geophysical anomalies indicating denser crust, which suggests present-day extension[113].

Active tectonic influences at mantle depths across Marie Byrd Land and the WA rift have been explored in the context of ice sheet modelling[114]. A slow seismic velocity anomaly (referred to as a 'plume') extends from

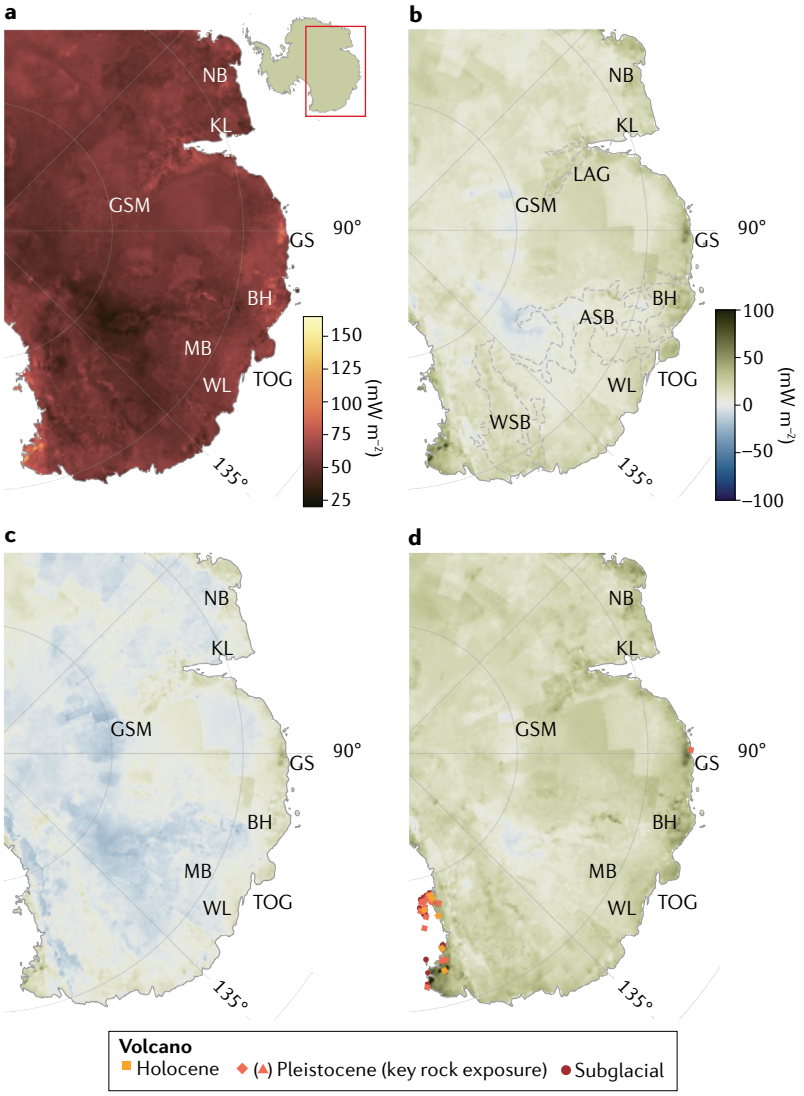

Fig. 4 | **East Antarctic GHF and anomalous components. a** | Aq1[17] multivariate empirical model from statistical similarity (same model as FIG. 2a). **b** | Difference between Aq1[17] and calculated solid state model, AqSS[20] (Aq1 – AqSS), with dotted lines showing the smoothed 500-m below sea level (bsl) contour in the subglacial topography (BEDMAP2[66]) to delineate the approximate location of subglacial basins. **c**,**d** | Panels **c** and **d** are companion plots to show consideration of uncertainties: **c**, smallest absolute difference between allowed values of Aq1 and AqSS models; **d**, largest absolute difference between allowed models, overlain by the locations of volcanoes. The range of values in Aq1 for East Antarctica is relatively small (the same colour scale as previous figures has been retained to avoid artificially enhancing slight changes in value[176]), and therefore features of interest can be more readily discerned in panel **b**. ASB, Aurora Subglacial Basin; BH, Bunger Hills; GS, Gaussberg; GSM, Gamburtsev Subglacial Mountains; KL, Kemp Land; LAG, Lambert–Amery Glacier; MB, Mawson block; NB, Napier block; WL, Wilkes Land; WSB, Wilkes Subglacial Basin; TOG, Totten Glacier. Differences between models can reveal anomalous components of GHF.

mid-mantle to the surface[115] indicating a higher potential temperature. Further consideration of the seismic wave speed anomalies[73,116,117] confirms the upper-mantle anomaly to be centred towards Marie Byrd land, and points to a complex interplay between composition, temperature and structure in the uppermost mantle and extended crust across Marie Byrd Land and the WA rift, noting relatively low incidence of tectonic-related seismic activity[118]. The longest-wavelength upper-mantle anomaly is likely to provide an elevated mantle heat contribution to the higher GHF differences in this region (seen in all models) including the adjacent WA rift. As an example, the exceptionally high GHF in the Thwaites Glacier region, and the lack of correlation with any single feature, suggest that the inferred GHF combines the effects of the upper-mantle anomaly, neotectonic rift, a cross-cutting (transform-type) fault zone[119] and topographic effects.

Lithospheric blocks of WA. The Marie Byrd Land dome shows moderately elevated Aq1 – AqSS model difference values that suggest stable but relatively young lithosphere, and features regional-scale faults[54,120] that have accommodated motion such as that occurring on the transform between Marie Byrd Land and Thurston Island[119]. Such faults can provide an additional mechanism for elevated heat flow[121]. The Ross Province subregion (FIG. 3b) is part of a separate tectonic province[58,120] but also shows regional-scale faulting. The Amundsen Province[58] (FIG. 3b, AMP) forms the northern and eastern part of the Marie Byrd Land dome[107] and features subdued topography with some exposed volcanoes. The greatly elevated central Marie Byrd Land has more exposed volcanoes[109,122] but comprises much less rock mass (that is, thicker ice) than previously thought[123] and is divided by the DeVicq Glacier and its deep trough. The Thurston Island block shows moderately elevated GHF difference values, matching a history of exhumation and uplift[124], and volcanic activity[109,122].

The Antarctic Peninsula shows finer detail in the pattern of GHF difference (some small elevated GHF patches) than other parts of WA, including high HPE intrusions of particular field interest compared with the country rocks[77]. The Haag and Ellsworth blocks have the appearance of stable lithosphere with the GHF model differences indicating conditions of steady state. Rock exposures include granites[54] with the potential for a substantial crustal contribution from high HPE[125]. The Ellsworth block appears similar to the lithosphere of EA in terms of both GHF, difference values and uncertainty characteristics.

Northern Victoria Land and Southern Victoria Land[126,127], part of the greater Transantarctic Mountains (FIG. 2), have exposed volcanoes (FIG. 3) and show elevated heat flow values in all models. In the case of Southern Victoria Land, Proterozoic and Palaeozoic basement is overlain by sedimentary and volcanic successions and a number of high-angle faults are inferred, cutting across Ross Orogen trends. The Ross Orogeny in Northern Victoria Land resulted from plate convergence and terrane accretion along the active margin of Gondwana. Inherited structures localize Cenozoic volcanic activity[109,128], adding components to the regional GHF.

East Antarctica

The pattern of mapped GHF, and model difference values for EA, depart only slightly from the predicted steady state model and confirm the overall picture of stable lithosphere. When comparing models for EA where the differences are subtle, the distinction between quantified and unquantified model uncertainties is especially relevant (Supplementary Note 3).

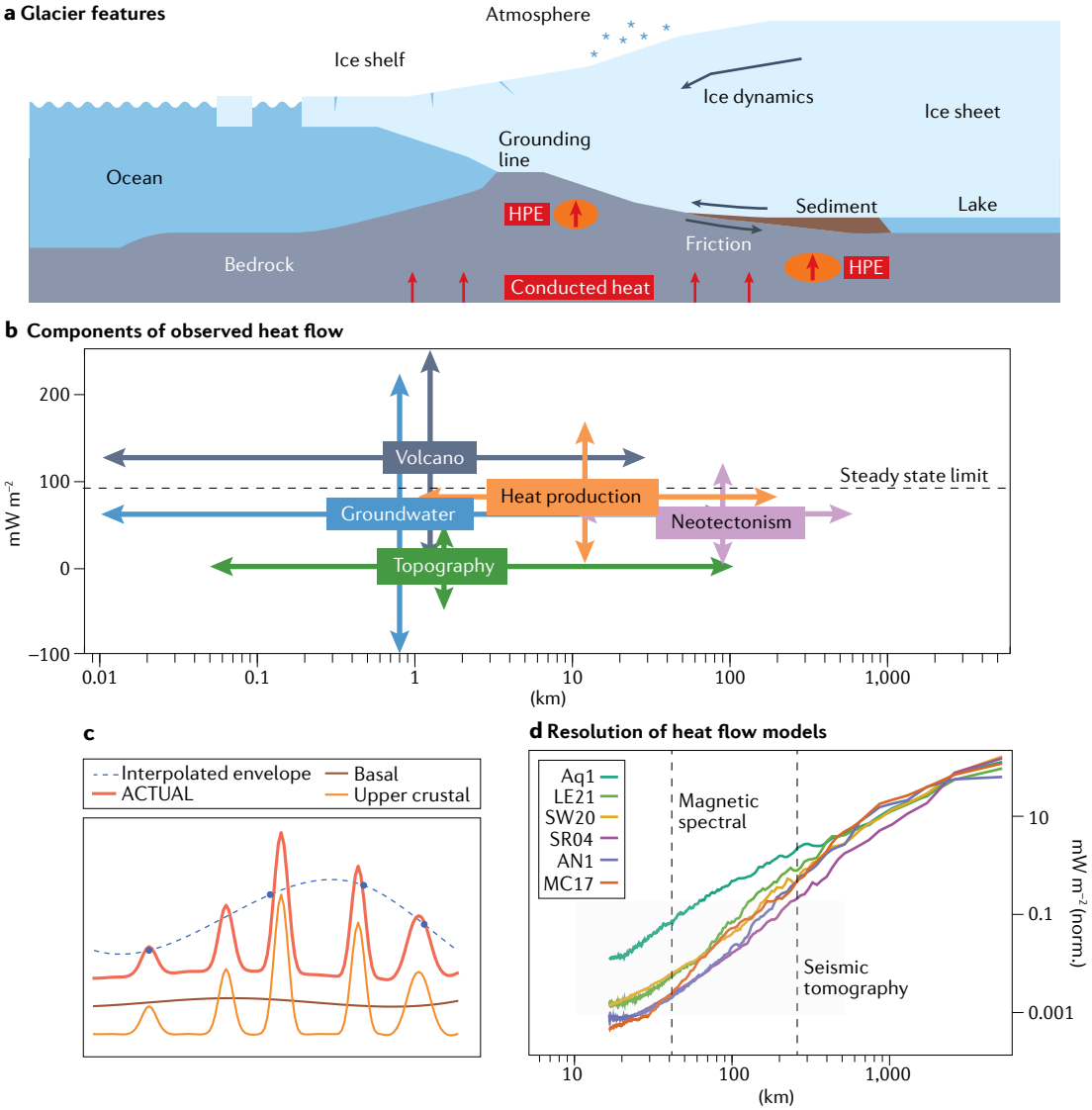

Fig. 5 | **The scale of various contributions to observed GHF. a** | Features of an outlet glacier system, where an ice sheet meets the ocean, showing influences on conditions at the ice sheet base: frictional heating and GHF. **b** | A plot showing the indicative magnitude and length scale of various mechanisms that can increase or reduce heat flow at a measured location, which includes volcanism, groundwater, topography, local heat production and neotectonism. The 90 mW m^{-2} line marks a suggested upper limit for a steady state condition, given the thermal conductivity and heat production of Earth's crust, and limits some forward models that are based on the temperature in the lithospheric mantle[76]. **c** | An indicative actual resultant GHF transect (thick red line) with a long-scale base component (thin brown line) and superposed shorter-scale upper-crustal component (thin orange line). Interpolating between sparse, isolated point GHF values (blue dots) could result in a falsely elevated GHF envelope (demonstrated with the dashed blue line). **d** | Power spectra of selected GHF models (background outlined in Supplementary Note 4). Some contributions to GHF are captured by the scale-length resolution of geophysical methods but some contributions are not resolved in detail.

South of 80° S and west of 45° E. The broad areas of elevated GHF values seen in EA in the central Transantarctic Mountains between the Ross Ice Shelf and the South Pole (FIG. 2; Aq1, LE21, SW20, SR04, FM05) could be linked to the slow seismic wavespeeds in the uppermost mantle identified beneath the Transantarctic Mountains and EA[129,130], noting that the region also hosts inferred high-angle faults[127]. The relatively high GHF anomaly close to the South Pole (Aq1 and LE21) is a robust regional-scale feature, but its exact form is not constrained, given the limited resolution of input datasets. Also indicated by englacial features in airborne radar[47], this anomaly is probably caused by HPE-enriched rock. Based on the probable subglacial geology and tectonic structure, some elevated GHF anomalies are likely to be present in many areas of EA.

Slightly elevated GHF values are seen in throughout Dronning Maud Land in the broad belt of Grenville-age (Meso- to Neoproterozoic) terranes that border the Archaean Grunehogna block and also the extensive region between the Grunehogna and Napier blocks[131] that includes Neoproterozoic oceanic arc terranes[132].

These observations follow the weak general correlation of GHF with tectonic age, with Proterozoic rocks having higher values than Archaean[33], noting the variations in continental heat production through time[29,32]. Low values are seen in the Archaean Grunehogna block (LE21 and SW20) and in the land areas bordering the southeast Weddell Sea. The trace of the border between these low values and the higher GHF of WA crosses the Weddell Sea coast further west than the usual boundary between EA and WA[62].

Exterior regions east of 45° E. The Napier block and the adjacent coast of Kemp Land comprise stable ancient lithosphere[56,133,134]. Low model differences would be expected for standard lithosphere, but slightly elevated values occur in these locations (FIG. 4b). Thin lithosphere, interpreted from seismic tomography models[73], provides a mechanism for the steady state GHF value to be higher than the subtracted AqSS value. Such elevated GHF difference values are shown around much of the EA coast and are also seen in model LE21.

The highest elevated GHF values (over 70 mW m^{-2} in Aq1) occur in the vicinity of Gaussberg volcano, active in the past 50–60 kyr (REF.[135]) and possibly part of a wider volcanic province[136]. This inference is made in a multivariate sense, and is not solely dependent on the presence of the volcano (Supplementary Note 2). Other influences on GHF could therefore also be important, including proximity to an interpreted major Gondwana-forming lithospheric boundary[71,137] and rift structures[138]. Late Neoproterozoic–Cambrian HPE-enriched suites are exposed along the Prydz Bay coast[56,91], probably intruded during Gondwana amalgamation processes[139]. In the Bunger Hills region, elevated GHF model difference values (FIG. 4b) could reflect such HPE-rich granitic plutons. Phanerozoic rift-related faults and basins[140,141] are also likely to be important in influencing the GHF distribution in this area, and into the interior.

Based on plate tectonic reconstructions of Gondwana[68,142,143], part of Wilkes Land has an affinity with southern Australia, which informs the interpretation of geophysical anomalies[69,144] and GHF along the Wilkes Land coast where crustal heat production dominates the regional GHF, and neotectonic processes have not subsequently overprinted the once-contiguous terranes[145]. The average GHF values in use for that part of EA are a reasonable match to the Australian counterparts, with the latter showing considerable variability beyond the resolution of the maps central to this review. Exhumation, erosion and deposition processes modify GHF[36]; hence, in the case of Antarctica, differences in landscape evolution compared with its Gondwanan neighbours[146,147] complicate GHF comparisons across conjugate margins.

Continental interior. South of 70°, a relatively low continental average (~55 mW m^{-2}, inferred from Aq1 in agreement with most other models) indicates a similarity with other regions of global continents where crustal heat production is extremely low, as is typical in Archaean and Palaeoproterozoic provinces[30]. This low average is consistent with vast tracts of ancient Precambrian crust across EA that are now at the surface[148–151] (or at the ice–bedrock interface) that exhibit crustal heat production values similar to global estimates[56]. The Gamburtsev Subglacial Mountains show slightly depressed values of GHF in Aq1 and more notable low values in LE21 (FIG. 2). Moraines from central EA show moderate heat production values[87] although local HPE-enriched sources are likely to be present (noting, for example, the 550–500 Ma granitoids[91] within Kuunga Orogen).

Sedimentary basins are not well mapped in EA, but could result in slightly raised or lowered GHF, depending on sediment provenance and age. The Lambert–Amery Glacier system catchment shows slightly elevated values corresponding with narrow, subglacial basin arms (FIG. 4b) and the Wilkes Subglacial Basin catchment also shows slightly elevated values corresponding with depressed subglacial topography. The Aurora Subglacial Basin and Wilkes Land[69,146] show relatively low values. These low values could be due to mature basin fill[68] with a low proportion of HPE (for example, quartz-arenite). Substantial parts of the Aurora Subglacial Basin could be acting as a thermal insulator owing to the low thermal conductivity of these materials, which could divert heat along bounding faults[42], although the resulting detail in the spatial pattern of GHF would be beyond the resolution of the continental-scale maps shown. The low GHF band between the Wilkes and Aurora Subglacial Basins is a feature of Aq1, although LE21 shows higher values in this location (FIG. 4, Supplementary Note 3).

Differences between GHF maps for Antarctica derived using alternative techniques have enabled some influences on GHF to be separated, which provides insight into past and present tectonic processes and influences on GHF.

Implications of GHF for ice sheets

Ice sheets flow under the force of gravity by the processes of deformation and basal sliding[6]. These processes depend on the ice sheet geometry (bed topography, ice thickness) and thermal regime, which in turn evolve in response to environmental forcing, for example, by surface temperature and precipitation. At the ice sheet base, frictional heating is the dominant heat source and boundary condition to the thermal model, particularly in fast-flowing glaciers or ice streams[152]. Groundwater flow is also of consequence in heat advection[153]. Geothermal heat is a secondary basal heat source, but often has high uncertainty, and has a greater effect for slow-moving ice[154]. In this section, the use of GHF as a boundary condition in ice sheet modelling is discussed. The accurate prediction of the quantity and timing of ice mass loss in locations that have been identified as vulnerable to irreversible loss, as tipping points in the global climate system, is a key goal of such modelling.

Scale lengths and GHF

GHF maps show anomalies at different scale lengths, partly owing to the depth of the source of the heat, and partly owing to the character of the source contribution. The scale length and the relative magnitude of the different anomalies contributing to observed heat flow can be compared to the features of an outlet glacier and its

associated ice sheet, the steady state limit of 90 mW m^{-2} (REF.[76]) and the spectral content of available GHF models (FIG. 5, Supplementary Note 4). The heat passing through the lithosphere represents the longest scale length component, which is added to by the heat produced or modified at shallower depths by numerous processes[155–157]. The GHF models for the Antarctic continent (FIG. 2) are able to represent the lithosphere component, the majority of neotectonism, and the longer wavelengths of the GHF impact of volcanoes; but are not able to capture a number of contributions to GHF likely to have an impact on ice sheets, such as the details of the crustal heat production. The scales of individual lithological units containing HPE can extend to much smaller scale lengths, and are of similar magnitude to the lithosphere component. Units high in HPE will hence form a peak in GHF superimposed on the baseline lithosphere component. Contributions from volcanoes and neotectonism potentially represent the highest values, and span a wide range. Contributions from groundwater can have positive or negative effects on the resulting GHF owing to the possibility of adding or removing heat. On the scale lengths relevant to outlet glaciers of ice sheets, the effect of HPE and possible refraction due to local subglacial topography on GHF anomalies can be at least as important as the regional GHF. Such fine-scale GHF anomalies have been shown to increase glacial melt estimates in an ice sheet model[158].

Heat transfer from bedrock to ice

At a continental scale, the GHF boundary condition is generally applied at a lower resolution than the scale of the topography at the ice–bed interface. At such low resolution, heat implicitly flows from the bed, into the ice, vertically. At finer resolution, this assumption breaks down: the topography between the bed and the ice above needs to be taken into consideration, as the direction of heat flow will refract (FIG. 1, BOX 1) according to the shape of the interface and the contrast in thermal conductivity between the rock and the ice[42,159]. The presence of gravel or other rock fragments in the ice will also influence its conductivity. Thermal conductivity measurements using a small sample of rock property values[160] do not capture some aspects of refraction effects, and these measurements should only be used in further quantitative research with caution. Applying a topographic correction is not straightforward because ice has a thermal conductivity value in the middle of the range of probable values for the underlying rock. Even if the subglacial topography is well constrained, then the lithology of the bedrock, and any faults or folds within the bedrock must be known to model the horizontal component of heat flow. Information on GHF from bedrock to ice can also be inferred from ice temperature profiles[39], noting the care required in interpreting single point measurements.

Tipping points in global systems

As global climate warms, the atmosphere and ocean forcing of the great ice sheets of Greenland and Antarctica will change. The response of ice sheets to changed forcings and Earth–ice feedbacks[3,161] are key research concerns because the resulting ice mass loss does not have a simple correlation to a value such as mean global temperature, but depends on the relative impact of glacier processes[162]. As an ice shelf thins slightly, it can be relatively stable, or lose contact with pinning points in the rock beneath[163] such that its ability to buttress upstream ice is weakened. In some locations, the impact could be widespread across a glacial catchment: for example, as an ice shelf retreats over retrograde bed topography it might expose thicker ice to ocean water, thus accelerating melting and further ice loss. Once a given retreat threshold is passed, the ice sheet will become unstable, and the collapse of part of the catchment will be inevitable and irreversible[164–166]. The most consequential of these thresholds are referred to as tipping points, and include glacier ice loss acceleration in WA, notably in the Thwaites Glacier region, and the Wilkes Subglacial Basin of EA[7]. The importance of tipping points is further extended owing to the compounding of uncertainties for interrelated components of the global climate system[8].

GHF as input to ice sheet models

Ice sheet modelling[6] is used to make a prediction regarding, or to test the importance of, some aspect of the ice sheet system. The boundary condition for the GHF part of the basal heat can be taken as the average value of GHF within a model cell, or polygon of a given size, together with a quantified uncertainty range. Depending on the extent of the ice sheet being investigated, it could be advisable not to clip the GHF model at the coastline. All the GHF models described in this Review could be used for this purpose, although those constrained by empirical methods would be preferred on a continental scale owing to the smaller impact of inherent assumptions (needed in all cases, noted in TABLE 1) on the salient features of the map. The use of ice sheet models to evaluate potential deep ice drill sites in Antarctica is one justification for why GHF must be known precisely[4]. Candidate sites[167] for obtaining extremely old ice cores (with basal layers dating to 1.5 Ma) in the attempt to resolve the mechanisms behind climate reorganization between 0.9 and 1.2 Ma have been identified at Dome Fuji and Dome C in East Antarctica.

Whereas early ice sheet models used a constant value for the GHF, many ice sheet models are now able to make use of a GHF boundary condition with a detailed spatial variability, opening up the possibility of testing the impact of a more realistic GHF distribution on the response of the ice sheet[168]. Ice sheet modelling experiments now simulate many alternative results across ranges of parameters, enabling an appraisal to be made of the ensemble of allowable results. Wider ice sheet model intercomparisons are also undertaken[169]. Owing to the generally low resolution of available GHF maps, simulation experiments have been used to test the impact of idealized, elevated GHF anomalies on ice dynamics in Antarctica. Localized patches of elevated GHF can accelerate ice flow upstream and downstream of the anomaly, with greater effect for slow-moving ice[170], and can substantially increase basal meltwater production that aids ice flow by basal sliding[114]. The impact of GHF on simulated ice flow is enhanced when a subglacial hydrology model is coupled to the ice dynamics[171].

When considering the most suitable form of the boundary condition for the GHF component of basal heat, the scale length and amplitude of high-GHF patches should be considered according to the probable form of intrusive bodies in the subglacial bedrock containing HPE. As noted previously, patches of high GHF can arise from HPE in the upper crust[91] or be related to fluids moving through fault zones[47,172]. Thus, generalized geological knowledge for a given region can help to bridge the gap between low-resolution GHF maps and an improved input to the ice sheet model that captures smaller scale lengths in the GHF component.

There is no satisfactory way to calculate a correction for refraction due to subglacial topography, and therefore the potential for horizontal components of GHF, unless the sub-ice shallow lithologies are known exactly and geological structure (including folds and faults) is constrained[42]. However, these impacts can be managed by assigning uncertainty to the GHF map used. At a local scale, if high-resolution airborne data are available, it is possible to use the form of englacial layers[173]. Given the potential to sample an unrepresentative GHF value due to HPE, hydrothermal or neotectonic processes, isolated GHF estimates based on in situ temperature measurements[40,41] should only be relied upon if the local context is understood.

GHF maps, tailored for use in ice sheet modelling, show spatially variable GHF values and can capture fine-scale anomalies within low and high bounds in the form of accompanying uncertainty maps.

Summary and future directions

The spatial variation of GHF can provide clues to the plate tectonic setting and tectonic history of Antarctica. However, complications arise as GHF is the result of sometimes numerous contributions at a given locality that can be difficult to distinguish. A comparison of Antarctic GHF maps and a consideration of scale lengths enables the separation of such influences.

The broad-scale GHF for West Antarctica is identified to vary in the range 59–119 mW m^{-2} (5th and 95th percentiles)[17], which is in broad agreement with other research that makes use of empirical methods and similarity based on global datasets[13,18]. Exceptionally high values of GHF occur in the region of the Thwaites Glacier, WA, where part of a mantle heat anomaly, a neotectonic rift, a cross-cutting (transform-type) fault zone[119], and the influence of subglacial topography beneath fast-flowing glaciers combine. Irreversible ice mass loss in this region has been identified as a possible tipping point in the global climate system[7]. Therefore, the pattern of GHF for the Thwaites Glacier region has important utility as a boundary condition for modelling to predict the present and future ice mass loss. In general, the GHF for WA inferred using global datasets is consistent with what might be anticipated based on geological structure[54] and GHF values based on direct measurements and glaciological observations[40,46]. More subtle elevated patches of GHF in many locations of WA are likely to be caused by intrusive lithologies in the upper crust with high concentrations of HPE.

The variation of GHF across East Antarctica is more subtle, across the range 45–66 mW m^{-2} (5th and 95th percentiles)[17], which is consistent with stable lithosphere that shows very little neotectonic influence. Slightly depressed GHF values occur in some interior locations that form the division between sedimentary basins. It is probable that other subtly elevated GHF anomalies are present within the model uncertainties for EA, and might yield further tectonic insights if they could be resolved. Yet, currently, many aspects of EA tectonics remain unresolved.

GHF models for Antarctica have now been developed by the research community that are low-resolution yet usable for continental-scale understanding of tectonic structure, and as boundary conditions for continental and catchment-scale ice sheet modelling. We recommend the use of a spatially variable GHF input with matching spatially variable uncertainty that captures the variance of input data and the assumptions inherent in the relevant methodology. In the immediate future, some refinements could be made to geophysical maps through model intercomparisons whereby methods[16–18] are applied to alternate datasets. Users should avoid arithmetic averaging of models inferred using different underlying methods, and instead use a quantitative process that yields fine-grained uncertainty and/or ranking of parameter metrics when combining constraints from different observables. With consideration for the underlying assumptions being made, models could be developed using joint constraints. Combining geophysical and glaciological constraints in a modelling framework is a high priority, given the interplay between glacier hydrology and basal conditions[45,167]. Further advances could be made in understanding the probable crustal component by undertaking HPE analyses of geological outcrop and transported samples held in national repositories to add to open-source compilations[56,57]. We concur with the need for ongoing sampling of rock outcrops for HPE and related analyses[15], and encourage field observations that would allow representative GHF transects[91] to be constructed to inform regional-scale research.

In the medium term, empirical GHF maps for Antarctica could be most improved through future field campaigns that provide better coverage of seismic stations across the continent. Tomographic maps of seismic properties have dual utility: they enable the empirical assignment of GHF values based on other observables (either using seismic data alone or as part of a multivariate set of constraining data), and they provide constraints on the nature of the lithosphere and mantle below. A further category of field data that would improve empirical GHF maps and progress knowledge with regard to the thermal structure of the continent of Antarctica is observables such as subglacial topography in databases such as Bedmap2[66], wherein vast areas still remain at low resolution. Improved resolution of topography would allow, for example, calculations related to thermal isostasy that are feasible for many continents but are weakly constrained for Antarctica.

We recommend that regional-scale GHF research and its applications should consider the likely amplitude and scale length of possible GHF anomalies based

on HPE content of lithologies in the upper crust and geological structure. Topography and/or variable geological structure and composition could introduce a horizontal component of GHF that can be accounted for through the use of spatially variable uncertainty bounds (supplied together with the relevant GHF model being used). Ice borehole estimates, of particular interest for high-heat-flow locations, should be obtained on an appropriate density grid of measurements, or else the context should be developed using supporting airborne geophysics or glacier observations at an appropriate resolution. Isolated determinations of GHF are unlikely to provide useful additional constraints for empirically or geophysically constrained heat flow maps unless the geological structure, groundwater conditions and rock thermal conductivity values are known[39,42].

The GHF of Antarctica remains a little-known property of a little-known continent; nevertheless, differences between alternative models are now better understood. Researchers now have access to empirical GHF results constrained by seismic or multivariate data. Such maps comprise central values with robust uncertainty bounds, which can be used as inputs to ongoing research, such as the ensemble-based ice sheet modelling that is important to predict the quantity and timing of Antarctic ice loss.

Data availability

The datasets analysed in this Review are available as open-source repositories (links below) or from the authors of the original studies. LE21[18] https://doi.org/10.1594/PANGAEA.930237; Aq1[17] https://doi.org/10.1594/PANGAEA.924857; AqSS[20] https://doi.org/10.1594/PANGAEA.918549; SW20[16] https://sites.google.com/view/weisen/research-products; GV20[174] available from authors of original article; MC17[74] https://doi.org/10.1594/PANGAEA.882503; AW15[76] http://www.seismolab.org/model/antarctica/lithosphere#an1-hf; FM05[75] http://websrv.cs.umt.edu/isis/index.php/Antarctica_Basal_Heat_Flux; SR04[13] available from authors of original article.

Published online: 26 October 2022

1. Fowler, C. M. R. *The Solid Earth: An Introduction to Global Geophysics* (Cambridge Univ. Press, 2004).
2. Jaupart, C. & Mareschal, J.-C. in *Treatise on Geophysics* 2nd edn, Vol. 6 (ed. Schubert, G.) 217–253 (Elsevier, 2015).
Detailed review covering many aspects of heat flow and the thermal structure of the lithosphere.
3. Whitehouse, P. L., Gomez, N., King, M. A. & Wiens, D. A. Solid Earth change and the evolution of the Antarctic Ice Sheet. *Nat. Commun.* **10**, 503 (2019).
4. Van Liefferinge, B. & Pattyn, F. Using ice-flow models to evaluate potential sites of million year-old ice in Antarctica. *Clim. Past.* **9**, 2335–2345 (2013).
5. Parnell, J. & McMahon, S. Physical and chemical controls on habitats for life in the deep subsurface beneath continents and ice. *Phil. Trans. R. Soc. A* **374**, 20140293 (2016).
6. Larour, E., Seroussi, H., Morlighem, M. & Rignot, E. Continental scale, high order, high spatial resolution, ice sheet modeling using the ice sheet system model (ISSM). *J. Geophys. Res. Earth Surf.* https://doi.org/10.1029/2011JF002140 (2012).
7. Lenton, T. M. et al. Climate tipping points — too risky to bet against. *Nature* https://doi.org/10.1038/d41586-019-03595-0 (2019).
8. Meredith, M. et al. in *Special Report on the Ocean and Cryosphere in a Changing Climate* (eds Pörtner, H.-O. et al.) Ch. 3 (IPCC, Cambridge Univ. Press, 2019).
9. Turcotte, D. & Schubert, M. *Geodynamics* (Cambridge Univ. Press, 2014).
10. Davies, J. H. Global map of solid Earth surface heat flow. *Geochem. Geophys. Geosyst.* **14**, 4608–4622 (2013).
11. Lucazeau, F. Analysis and mapping of an updated terrestrial heat flow data set. *Geochem. Geophys. Geosyst.* **20**, 4001–4024 (2019).
Analysis of a global dataset including quantitative support for representative values in different tectonic settings, and uncertainty estimates.
12. Stål, T. et al. Properties and biases of the global heat flow compilation. *Front. Earth Sci.* https://doi.org/10.3389/feart.2022.963525 (2022).
13. Shapiro, N. M. & Ritzwoller, M. H. Inferring surface heat flux distributions guided by a global seismic model: particular application to Antarctica. *Earth Planet. Sci. Lett.* **223**, 213–224 (2004).
14. Li, C. F., Lu, Y. & Wang, J. A global reference model of Curie-point depths based on EMAG2. *Sci. Rep.* **7**, 45129 (2017).
15. Burton-Johnson, A., Dziadek, R. & Martin, C. Geothermal heat flow in Antarctica: current and future directions. *Cryosphere* https://doi.org/10.5194/tc-2020-59 (2020).
Review of geothermal heat flow (GHF) in Antarctica of broad scope that includes glaciological, geophysical, geological and marine geoscience approaches.
16. Shen, W., Wiens, D. A., Lloyd, A. J. & Nyblade, A. A. A geothermal heat flux map of Antarctica empirically constrained by seismic structure. *Geophys. Res. Lett.* **47**, 0–2 (2020).
GHF of Antarctica modelled on high quality datasets from the USA using seismic tomography and a similarity approach.
17. Stål, T., Reading, A. M., Halpin, J. A. & Whittaker, J. M. Antarctic geothermal heat flow model: Aq1. *Geochem. Geophys. Geosyst.* **22**, e2020GC009428 (2021).
GHF of Antarctica modelled on global datasets using a refined similarity approach.
18. Lösing, M. & Ebbing, J. Predicting geothermal heat flow in Antarctica with a machine learning approach. *J. Geophys. Res. Solid Earth* **126**, e2020JB021499 (2021).
GHF of Antarctica modelled on global datasets using a machine learning approach.
19. Stål, T. & Reading, A. M. A grid for multidimensional and multivariate spatial representation and data processing. *J. Open. Res. Softw.* **8**, https://doi.org/10.5334/jors.287 (2020).
20. Stål, T., Reading, A. M., Halpin, J. A., Steven J, P. & Whittaker, J. M. The Antarctic crust and upper mantle: a flexible 3D model and framework for interdisciplinary research. *Front. Earth Sci.* https://doi.org/10.3389/feart.2020.577502 (2020).
A computational framework that enables model calculation and comparison.
21. Burton-Johnson, A., Black, M., Peter, T. F. & Kaluza-Gilbert, J. An automated methodology for differentiating rock from snow, clouds and sea in Antarctica from Landsat 8 imagery: a new rock outcrop map and area estimation for the entire Antarctic continent. *Cryosphere* **10**, 1665–1677 (2016).
22. Foulger, G. R., Lustrino, M. & King, S. D. *The Interdisciplinary Earth: A Volume in Honor of Don L. Anderson* (Geological Society of America, 2015).
23. Lay, T., Hernlund, J. & Buffett, B. A. Core–mantle boundary heat flow. *Nat. Geosci.* **1**, 25–32 (2008).
24. Dye, S. Geoneutrinos and the radioactive power of the Earth. *Rev. Geophys.* https://doi.org/10.1029/2012RG000400 (2012).
25. Arevalo, R., McDonough, W. F. & Luong, M. The K/U ratio of the silicate earth: insights into mantle composition, structure and thermal evolution. *Earth Planet. Sci. Lett.* **278**, 361–369 (2009).
26. Chapman, D. S. Thermal gradients in the continental crust. *Geol. Soc. Spec. Publ.* **24**, 63–70 (1986).
27. Goutorbe, B., Poort, J., Lucazeau, F. & Raillard, S. Global heat flow trends resolved from multiple geological and geophysical proxies. *Geophys. J. Int.* **187**, 1405–1419 (2011).
28. Artemieva, I. M., Thybo, H., Jakobsen, K., Sorensen, N. K. & Nielsen, L. S. Heat production in granitic rocks: global analysis based on a new data compilation. *Earth Sci. Rev.* **172**, 1–26 (2017).
29. Hasterok, D., Gard, M., Cox, G. & Hand, M. A 4 Ga record of granitic heat production: implications for geodynamic evolution and crustal composition of the early Earth. *Precambrian Res.* **331**, 105375 (2019).
30. Jaupart, C., Mareschal, J. C. & Iarotsky, L. Radiogenic heat production in the continental crust. *Lithos* **262**, 398–427 (2016).
31. Gard, M., Hasterok, D. & Halpin, J. A. Global whole-rock geochemical database compilation. *Earth Syst. Sci. Data* **11**, 1553–1566 (2019).
32. Gard, M., Hasterok, D., Hand, M. & Cox, G. Variations in continental heat production from 4 Ga to the present: evidence from geochemical data. *Lithos* **342–343**, 391–406 (2019).
33. Goes, S., Hasterok, D., Schutt, D. L. & Klocking, M. Continental lithospheric temperatures: a review. *Phys. Earth Planet. Inter.* **306**, 106509 (2020).
34. Hacker, B. R., Kelemen, P. B. & Behn, M. D. Differentiation of the continental crust by relamination. *Earth Planet. Sci. Lett.* **307**, 501–516 (2011).
35. Rudnick, R. L. & Gao, S. Composition of the continental crust. *Treatise Geochem.* **4**, 1–51 (2014).
36. Beardsmore, G. R. & Cull, J. P. *Crustal Heat Flow* (Cambridge Univ. Press, 2001).
37. Lees, C. H. On the shapes of the isogeotherms under mountain ranges in radio-active districts. *Proc. R. Soc. Lond. A* **83**, 339–346 (1910).
38. Slagstad, T., Midttømme, K., Ramstad, R. K. & Slagstad, D. Factors influencing shallow (<1000 m depth) temperatures and their significance for extraction of ground-source heat. *Geol. Soc. Spec. Publ.* **11**, 99–109 (2008).
39. Mony, L., Roberts, J. L. & Halpin, J. A. Inferring geothermal heat flux from an ice-borehole temperature profile at Law Dome, East Antarctica. *J. Glaciol.* **66**, 509–519 (2020).
40. Fisher, A. T., Mankoff, K. D., Tulaczyk, S. M., Tyler, S. W. & Foley, N. High geothermal heat flux measured below the West Antarctic Ice Sheet. *Sci. Adv.* https://doi.org/10.1126/sciadv.1500093 (2015).
41. Begeman, C. B., Tulaczyk, S. M. & Fisher, A. T. Spatially variable geothermal heat flux in West Antarctica: evidence and implications. *Geophys. Res. Lett.* **44**, 9823–9832 (2017).
42. Willcocks, S., Hasterok, D. & Jennings, S. Thermal refraction: implications for subglacial heat flux. *J. Glaciol.* **67**, 875–884 (2021).
An exploration of GHF anomalies owing to refraction of heat associated with subglacial topography and contrasts in the thermal properties of geological materials.
43. Pattyn, F. Antarctic subglacial conditions inferred from a hybrid ice sheet/ice stream model. *Earth Planet. Sci. Lett.* **295**, 451–461 (2010).

44. Siegert, M. J. et al. Antarctic subglacial groundwater: a concept paper on its measurement and potential influence on ice flow. *Geol. Soc. Spec. Publ.* **461**, 197–213 (2018).
45. Dow, C. et al. Totten glacier subglacial hydrology determined from geophysics and modeling. *Earth Planet. Sci. Lett.* **531**, 115961 (2020).
46. Schroeder, D. M., Blankenship, D. D., Young, D. A. & Quartini, E. Evidence for elevated and spatially variable geothermal flux beneath the West Antarctic Ice Sheet. *Proc. Natl Acad. Sci. USA* **111**, 9070–9072 (2014).
47. Jordan, T. A. et al. Anomalously high geothermal flux near the South Pole. *Sci. Rep.* **8**, 16785 (2018).
48. Kerr, Y. H. et al. The SMOS mission: new tool for monitoring key elements of the global water cycle. *Proc. IEEE* **98**, 666–687 (2010).
49. Livingstone, S. J. et al. Subglacial lakes and their changing role in a warming climate. *Nat. Rev. Earth Environ.* https://doi.org/10.1038/s43017-021-00246-9 (2022).
50. Passalacqua, O. et al. Retrieval of the absorption coefficient of L-band radiation in Antarctica from SMOS observations. *Remote Sens.* https://doi.org/10.3390/rs10121954 (2018).
51. Macelloni, G. et al. On the retrieval of internal temperature of Antarctica Ice Sheet by using SMOS observations. *Remote. Sens. Environ.* **233**, 111405 (2019).
52. Fudge, T. J., Biyani, S. C., Clemens-Sewall, D. & Hawley, R. L. Constraining geothermal flux at coastal domes of the Ross Ice Sheet, Antarctica. *Geophys. Res. Lett.* **46**, 13090–13098 (2019).
53. Kleinschmidt, G. (ed.) *The Geology of the Antarctic Continent* (Schweizerbart Science, 2021).
54. Jordan, T. A., Riley, T. R. & Siddoway, C. S. The geological history and evolution of West Antarctica. *Nat. Rev. Earth Environ.* **1**, 117–133 (2020).
Review paper on the geology and tectonic evolution of West Antarctica.
55. Harley, S. L., Fitzsimons, I. C. & Zhao, Y. Antarctica and supercontinent evolution: historical perspectives, recent advances and unresolved issues. *Geol. Soc. Spec. Publ.* **383**, 1–34 (2013).
Review paper on the geology and tectonic evolution of East Antarctica.
56. Sanchez, G. et al. PetroChron Antarctica: a geological database for interdisciplinary use. *Geochem. Geophys. Geosyst.* https://doi.org/10.1029/2021GC010154 (2021).
57. Cox, S. C., Smith Lyttle, B. & the GeoMAP team. *ATA SCAR GeoMAP geology* (v.2022-08)(GNS Science, 2022); https://doi.org/10.21420/7SH-6K05.
58. Siddoway, C. in *The Geology of the Antarctic Continent* (ed. Kleinschmidt, G.) 87–131 (Schweizerbart Science, 2021).
59. Argus, D. F., Peltier, W. R., Drummond, R. & Moore, A. W. The Antarctica component of postglacial rebound model ICE-6G_C (VM5a) based on GPS positioning, exposure age dating of ice thicknesses, and relative sea level histories. *Geophys. J. Int.* **198**, 537–563 (2014).
60. Shen, W. et al. The crust and upper mantle structure of Central and West Antarctica from Bayesian inversion of Rayleigh wave and receiver functions. *J. Geophys. Res. Solid Earth* **123**, 7824–7849 (2018).
61. Smellie, J. in *The Geology of the Antarctic Continent* (ed. Kleinschmidt, G.) 18–86 (Schweizerbart Science, 2021).
62. Artemieva, I. M. & Thybo, H. Continent size revisited: geophysical evidence for West Antarctica as a back-arc system. *Earth Sci. Rev.* **202**, 103106 (2020).
63. Boger, S. D. Antarctica — before and after Gondwana. *Gondwana Res.* **19**, 335–371 (2011).
64. Turner, R. J., Reading, A. M. & King, M. A. Separation of tectonic and local components of horizontal GPS station velocities: a case study for glacial isostatic adjustment in East Antarctica. *Geophys. J. Int.* **222**, 1555–1569 (2020).
65. Ferraccioli, F. et al. East Antarctic rifting triggers uplift of the Gamburtsev Mountains. *Nature* **479**, 388–392 (2011).
66. Fretwell, P. et al. Bedmap2: improved ice bed, surface and thickness datasets for Antarctica. *Cryosphere* **6**, 4305–4361 (2012).
67. Morlighem, M. et al. Deep glacial troughs and stabilizing ridges unveiled beneath the margins of the Antarctic ice sheet. *Nat. Geosci.* https://doi.org/10.1038/s41561-019-0510-8 (2019).
68. Maritati, A., Halpin, J. A., Whittaker, J. M. & Daczko, N. R. Fingerprinting Proterozoic bedrock in interior Wilkes Land, East Antarctica. *Sci. Rep.* **9**, 10192 (2019).
69. Aitken, A. R. et al. The subglacial geology of Wilkes Land, East Antarctica. *Geophys. Res. Lett.* **41**, 2390–2400 (2014).
70. Stål, T., Reading, A. M., Halpin, J. A. & Whittaker, J. M. A multivariate approach for mapping lithospheric domain boundaries in East Antarctica. *Geophys. Res. Lett.* **46**, 10404–10416 (2019).
71. Mulder, J. A. et al. A multiproxy provenance approach to uncovering the assembly of East Gondwana in Antarctica. *Geology* **47**, 645–649 (2019).
72. Dziadek, R., Ferraccioli, F. & Gohl, K. High geothermal heat flow beneath Thwaites Glacier in West Antarctica inferred from aeromagnetic data. *Commun. Earth Environ.* **2**, 162 (2021).
73. Lloyd, A. J. et al. Seismic structure of the Antarctic upper mantle imaged with adjoint tomography. *J. Geophys. Res. Solid Earth* **125**, 2019JB017823 (2020).
74. Martos, Y. M. et al. Heat flux distribution of Antarctica unveiled. *Geophys. Res. Lett.* **44**, 11417–11426 (2017).
75. Fox Maule, C., Purucker, M. E., Olsen, N. & Mosegaard, K. Heat flux anomalies in Antarctica revealed by satellite magnetic data. *Science* **309**, 464–467 (2005).
76. An, M. et al. Temperature, lithosphere-asthenosphere boundary, and heat flux beneath the Antarctic Plate inferred from seismic velocities. *J. Geophys. Res. Solid Earth* **120**, 8720–8742 (2015).
77. Burton-Johnson, A., Halpin, J. A., Whittaker, J. M., Graham, F. S. & Watson, S. J. A new heat flux model for the Antarctic Peninsula incorporating spatially variable upper crustal radiogenic heat production. *Geophys. Res. Lett.* **44**, 5436–5446 (2017).
78. Ebbing, J., Gernigon, L., Pascal, C., Olesen, O. & Osmundsen, P. T. A discussion of structural and thermal control of magnetic anomalies on the mid-Norwegian margin. *Geophys. Prospect.* **57**, 665–681 (2009).
79. Gard, M. & Hasterok, D. A global Curie depth model utilising the equivalent source magnetic dipole method. *Phys. Earth Planet. Inter.* **313**, 106672 (2021).
80. An, M. et al. S-velocity model and inferred Moho topography beneath the Antarctic Plate from Rayleigh waves. *J. Geophys. Res. Solid. Earth* **120**, 359–383 (2015).
81. Goes, S., Govers, R. & Vacher, P. Shallow mantle temperatures under Europe from P and S wave tomography. *J. Geophys. Res. Solid Earth* **105**, 11153–11169 (2000).
82. An, M. & Shi, Y. Three-dimensional thermal structure of the Chinese continental crust and upper mantle. *Sci. China D Earth Sci.* **50**, 1441–1451 (2007).
83. Haeger, C., Kaban, M. K., Tesauro, M., Petrunin, A. G. & Mooney, W. D. 3-D density, thermal, and compositional model of the Antarctic lithosphere and implications for its evolution. *Geochem. Geophys. Geosyst.* **20**, 688–707 (2019).
84. Schaeffer, A. J. & Lebedev, S. Global shear speed structure of the upper mantle and transition zone. *Geophys. J. Int.* **194**, 417–449 (2013).
85. Lösing, M., Ebbing, J. & Szwillus, W. Geothermal heat flux in Antarctica: assessing models and observations by Bayesian inversion. *Front. Earth Sci.* https://doi.org/10.3389/feart.2020.00105 (2020).
Assessment of the influence of different lithospheric models on heat flow calculations for Antarctica.
86. Hasterok, D., Gard, M. & Webb, J. On the radiogenic heat production of metamorphic, igneous, and sedimentary rocks. *Geosci. Front.* **9**, 1777–1794 (2018).
Appraisal of radiogenic heat production in upper crustal rocks.
87. Goodge, J. W. Crustal heat production and estimate of terrestrial heat flow in central East Antarctica, with implications for thermal input to the East Antarctic ice sheet. *Cryosphere* **12**, 491–504 (2018).
88. Aitken, A. & Urosevic, L. A probabilistic and model-based approach to the assessment of glacial detritus from ice sheet change. *Palaeogeogr. Palaeoclimatol. Palaeoecol.* **561**, 110053 (2021).
89. Venzke, E. (ed.) in *Volcanoes of the World* v. 4.9.0., https://doi.org/10.5479/si.GVP.VOTW4-2013 (Smithsonian Institution, 2013).
90. Schaeffer, A. J. & Lebedev, S. in *Earth's Heterogeneous Mantle*, 3–46 (Springer, 2015).
91. Carson, C. J., McLaren, S., Roberts, J. L., Boger, S. D. & Blankenship, D. D. Hot rocks in a cold place: high sub-glacial heat flow in East Antarctica. *J. Geol. Soc.* **171**, 9–12 (2014).
92. Mongelli, F. & Zito, G. The contemporary effect of erosion/sedimentation and past climate on the geothermal gradient. *Stud. Geophys. Geod.* **37**, 258–264 (1993).
93. Cammarano, F., Goes, S., Vacher, P. & Giardini, D. Inferring upper-mantle temperatures from seismic velocities. *Phys. Earth Planet. Inter.* **138**, 197–222 (2003).
94. Kaban, M. K., Tesauro, M., Mooney, W. D. & Cloetingh, S. A. P. L. Density, temperature, and composition of the North American lithosphere — new insights from a joint analysis of seismic, gravity, and mineral physics data: 1. Density structure of the crust and upper mantle. *Geochem. Geophys. Geosyst.* **15**, 4781–4807 (2014).
95. Afonso, J. C., Salajegheh, F., Szwillus, W., Ebbing, J. & Gaina, C. A global reference model of the lithosphere and upper mantle from joint inversion and analysis of multiple data sets. *Geophys. J. Int.* **217**, 1602–1628 (2019).
96. Sammon, L. G., Gao, C. & McDonough, W. F. Lower crustal composition in the southwestern United States. *J. Geophys. Res. Solid Earth* **125**, e2019JB019011 (2020).
97. Sui, S., Shen, W., Schulte-Pelkum, V. & Mahan, K. Constraining the crustal composition of the continental U.S. using seismic observables. *GSA Bull.* (in the press).
98. Pappa, F., Ebbing, J., Ferraccioli, F. & van der Wal, W. Modeling satellite gravity gradient data to derive density, temperature, and viscosity structure of the Antarctic lithosphere. *J. Geophys. Res. Solid Earth* **124**, 12053–12076 (2019).
99. Hasterok, D. & Gard, M. Utilizing thermal isostasy to estimate sub-lithospheric heat flow and anomalous crustal radioactivity. *Earth Planet. Sci. Lett.* **450**, 197–207 (2016).
100. Artemieva, I. M. Antarctica ice sheet basal melting enhanced by high mantle heat. *Earth Sci. Rev.* **226**, 103954 (2022).
101. Stevens, N. T., Parizek, B. R. & Alley, R. B. Enhancement of volcanism and geothermal heat flux by ice-age cycling: a stress modeling study of Greenland. *J. Geophys. Res. Earth Surf.* **121**, 1456–1471 (2016).
102. Diao, N., Li, Q. & Fang, Z. Heat transfer in ground heat exchangers with groundwater advection. *Int. J. Therm. Sci.* **43**, 1203–1211 (2004).
103. Cracknell, M. J. & Reading, A. M. The upside of uncertainty: identification of lithology contact zones from airborne geophysics and satellite data using random forests and support vector machines. *Geophysics* **78**, WB113–WB126 (2013).
104. Wellmann, J. F. Information theory for correlation analysis and estimation of uncertainty reduction in maps and models. *Entropy* **15**, 1464–1485 (2013).
105. Jaupart, C. & Mareschal, J. C. in *Treatise on Geochemistry* 2nd edn, Vol. 4, 53–73 (Elsevier, 2013).
106. Behrendt, J. C. Crustal and lithospheric structure of the West Antarctic Rift System from geophysical investigations — a review. *Glob. Planet. Change* **23**, 25–44 (1999).
107. Siddoway, C. S. in *Antarctica: A Keystone in a Changing World* (eds Cooper, A. K. et al.) (National Academies Press, 2008); https://doi.org/10.3133/ofr20071047KP09.
108. Scambos, T. et al. How much, how fast? A science review and outlook for research on the instability of Antarctica's Thwaites Glacier in the 21st century. *Glob. Planet. Change* **153**, 16–34 (2017).
109. van Wyk de Vries, M., Bingham, R. G. & Hein, A. S. A new volcanic province: an inventory of subglacial volcanoes in West Antarctica. *Geol. Soc. Spec. Publ.* **461**, 231–248 (2018).
110. Bell, R. E. et al. Influence of subglacial geology on the onset of a West Antarctic ice stream from aerogeophysical observations. *Nature* **394**, 58–62 (1998).
111. Bell, R., Studinger, M., Karner, G., Finn, C. & Blankenship, D. in *Antarctica* (eds Fütterer, D. et al.) 117–121 (Springer, 2006).
112. Behrendt, J. C. et al. Patterns of late Cenozoic volcanic and tectonic activity in the West Antarctic rift system revealed by aeromagnetic surveys. *Tectonics* **15**, 660–676 (1996).
113. Tankersley, M. D., Horgan, H. J., Siddoway, C. S., Caratori Tontini, F. & Tinto, K. J. Basement topography and sediment thickness beneath Antarctica's Ross Ice Shelf. *Geophys. Res. Lett.* **49**, e2021GL097371 (2022).
114. Seroussi, H., Ivins, E. R., Wiens, D. A. & Bondzio, J. Influence of a West Antarctic mantle plume on ice sheet basal conditions. *J. Geophys. Res. Solid Earth* **122**, 7127–7155 (2017).

115. Hansen, S. E. et al. Imaging the Antarctic mantle using adaptively parameterized P-wave tomography: evidence for heterogeneous structure beneath West Antarctica. *Earth Planet. Sci. Lett.* **408**, 66–78 (2014).
116. O'Donnell, J. P. et al. The uppermost mantle seismic velocity structure of West Antarctica from Rayleigh wave tomography: insights into tectonic structure and geothermal heat flow. *Earth Planet. Sci. Lett.* **522**, 219–233 (2019).
117. Lucas, E. M. et al. P- and S-wave velocity structure of central West Antarctica: implications for the tectonic evolution of the West Antarctic Rift System. *Earth Planet. Sci. Lett.* **546**, 116437 (2020).
118. Lucas, E. M. et al. Seismicity and Pn velocity structure of Central West Antarctica. *Geochem. Geophys. Geosyst.* **22**, e2020GC009471 (2021).
119. Muller, R. D., Gohl, K., Cande, S. C., Goncharov, A. & Golynsky, A. V. Eocene to Miocene geometry of the West Antarctic Rift System. *Aust. J. Earth Sci.* **54**, 1033–1045 (2007).
120. Zundel, M., Spiegel, C., Lisker, F. & Monien, P. Post mid-Cretaceous tectonic and topographic evolution of Western Marie Byrd Land, West Antarctica: insights from apatite fission track and (U-Th-Sm)/He data. *Geochem. Geophys. Geosyst.* **20**, 5831–5848 (2019).
121. Duwiquet, H., Arbaret, L., Guillou-Frottier, L., Heap, M. J. & Bellanger, M. On the geothermal potential of crustal fault zones: a case study from the Pontgibaud area (French Massif Central, France). *Geotherm. Energy* **7**, 33 (2019).
122. Wilch, T. I., McIntosh, W. C. & Panter, K. S. Chapter 5.4a Marie Byrd Land and Ellsworth Land: volcanology. *Geol. Soc. Lond. Mem.* **55**, 515–576 (2021).
123. Holschuh, N., Pollard, D., Alley, R. & Anandakrishnan, S. Evaluating Marie Byrd Land stability using an improved basal topography. *Earth Planet. Sci. Lett.* **408**, 362–369 (2014).
124. Zundel, M. et al. Thurston Island (West Antarctica) between Gondwana subduction and continental separation: a multistage evolution revealed by apatite thermochronology. *Tectonics* **38**, 878–897 (2019).
125. Leat, P. T. et al. Jurassic high heat production granites associated with the Weddell Sea rift system, Antarctica. *Tectonophysics* **722**, 249–264 (2018).
126. Goodge, J. W. Geological and tectonic evolution of the Transantarctic Mountains, from ancient craton to recent enigma. *Gondwana Res.* **80**, 50–122 (2020).
127. Goodge, J. in *The Geology of the Antarctic Continent* (ed. Kleinschmidt, G.) 132–217 (Schweizerbart Science, 2021).
128. Smellie, J. L. & Rocchi, S. Chapter 5.1a. Northern Victoria Land: volcanology. *Geol. Soc. Lond. Mem.* **55**, 347–381 (2021).
129. Brenn, G. R., Hansen, S. E. & Park, Y. Variable thermal loading and flexural uplift along the Transantarctic Mountains, Antarctica. *Geology* **45**, 463–466 (2017).
130. Shen, W. et al. Seismic evidence for lithospheric foundering beneath the southern Transantarctic Mountains, Antarctica. *Geology* **46**, 71–74 (2017).
131. Läufer, A. in *The Geology of the Antarctic Continent* (ed. Kleinschmidt, G.) 254–295 (Schweizerbart Science, 2021).
132. Ruppel, A., Jacobs, J., Eagles, G., Läufer, A. & Jokat, W. New geophysical data from a key region in East Antarctica: estimates for the spatial extent of the Tonian Oceanic Arc Super Terrane (TOAST). *Gondwana Res.* **59**, 97–107 (2018).
133. Black, L., Sheraton, J. & James, P. Late Archaean granites of the Napier Complex, Enderby Land, Antarctica: a comparison of Rb-Sr, Sm-Nd and U-Pb isotopic systematics in a complex terrain. *Precambrian Res.* **32**, 343–368 (1986).
134. Halpin, J., Gerakiteys, C., Clarke, G., Belousova, E. & Griffin, W. In-situ U–Pb geochronology and Hf isotope analyses of the Rayner Complex, east Antarctica. *Contrib. Mineral. Petrol.* **148**, 689–706 (2005).
135. Tingey, R. J., McDougall, I. & Gleadow, A. J. W. The age and mode of formation of Gaussberg, Antarctica. *J. Geol. Soc. Aust.* **30**, 241–246 (1983).
136. Smellie, J. L. & Collerson, K. D. Chapter 5.5. Gaussberg: volcanology and petrology. *Geol. Soc. Lond. Mem.* https://doi.org/10.1144/M55-2018-85 (2021).
137. Daczko, N. R., Halpin, J. A., Fitzsimons, I. C. W. & Whittaker, J. M. A cryptic Gondwana-forming orogen located in Antarctica. *Sci. Rep.* **8**, 8371 (2018).
138. Ferraccioli, F. et al. Gaussberg rift — illusion or reality? In *Antarctica: A Keystone in a Changing World – Online Proceedings of the 10th ISAES X* (eds Cooper, A. K. et al.) USGS Open-File Report 2007-1047, 1996 (US Geological Survey and The National Academies, 2007).
139. Halpin, J. A., Daczko, N. R., Kobler, M. E. & Whittaker, J. M. Strike-slip tectonics during the Neoproterozoic–Cambrian assembly of East Gondwana: evidence from a newly discovered microcontinent in the Indian Ocean (Batavia Knoll). *Gondwana Res.* **51**, 137–148 (2017).
140. Maritati, A. et al. The tectonic development and erosion of the Knox Subglacial Sedimentary Basin, East Antarctica. *Geophys. Res. Lett.* **43**, 10728–10737 (2016).
141. Maritati, A., Danisik, M., Halpin, J. A., Whittaker, J. M. & Aitken, A. R. A. Pangea rifting shaped the East Antarctic landscape. *Tectonics* **39**, e2020TC006180 (2020).
142. Aitken, A. et al. The Australo-Antarctic Columbia to Gondwana transition. *Gondwana Res.* **29**, 136–152 (2016).
143. Williams, S. E., Whittaker, J. M., Halpin, J. A. & Muller, R. D. Australian-Antarctic breakup and seafloor spreading: balancing geological and geophysical constraints. *Earth Sci. Rev.* **188**, 41–58 (2019).
144. Ebbing, J., Dilixiati, Y., Haas, P., Ferraccioli, F. & Scheiber-Enslin, S. East Antarctica magnetically linked to its ancient neighbours in Gondwana. *Sci. Rep.* **11**, 5513 (2021).
145. Pollett, A. et al. Heat flow in Southern Australia and connections with East Antarctica. *Geochem. Geophys. Geosyst.* **20**, 5352–5370 (2019).
146. Paxman, G. J. et al. Reconstructions of Antarctic topography since the Eocene–Oligocene boundary. *Palaeogeogr. Palaeoclimatol. Palaeoecol.* **535**, 109346 (2019).
147. Sauermilch, I., Whittaker, J. M., Bijl, P. K., Totterdell, J. M. & Jokat, W. Tectonic, oceanographic, and climatic controls on the Cretaceous-Cenozoic sedimentary record of the Australian-Antarctic Basin. *J. Geophys. Res. Solid Earth* **124**, 7699–7724 (2019).
148. Duclaux, G. et al. Superimposed Neoarchaean and Paleoproterozoic tectonics in the Terre Adélie Craton (East Antarctica): evidence from Th–U–Pb ages on monazite and $^{40}Ar/^{39}Ar$ ages. *Precambrian Res.* **167**, 316–338 (2008).
149. Halpin, J. A., White, R. W., Clarke, G. L. & Kelsey, D. E. The Proterozoic *P–T–t* evolution of the Kemp Land Coast, East Antarctica; constraints from Si-saturated and Si-undersaturated metapelites. *J. Petrol.* **48**, 1321–1349 (2007).
150. Morrissey, L. J., Hand, M. & Kelsey, D. E. Multi-stage metamorphism in the Rayner–Eastern Ghats Terrane: *P–T–t* constraints from the northern Prince Charles Mountains, east Antarctica. *Precambrian Res.* **267**, 137–163 (2015).
151. Tucker, N. M. et al. Proterozoic reworking of Archean (Yilgarn) basement in the Bunger Hills, East Antarctica. *Precambrian Res.* **298**, 16–38 (2017).
152. Leysinger Vieli, G. J.-M. C., Martín, C., Hindmarsh, R. C. A. & Lüthi, M. P. Basal freeze-on generates complex ice-sheet stratigraphy. *Nat. Commun.* **9**, 4669 (2018).
153. Gooch, B. T., Young, D. A. & Blankenship, D. D. Potential groundwater and heterogeneous heat source contributions to ice sheet dynamics in critical submarine basins of East Antarctica. *Geochem. Geophys. Geosyst.* **17**, 395–409 (2016).
154. Llubes, M., Lanseau, C. & Remy, F. Relations between basal condition, subglacial hydrological networks and geothermal flux in Antarctica. *Earth Planet. Sci. Lett.* **241**, 655–662 (2006).
155. Davies, J. H. & Davies, D. R. Earth's surface heat flux. *Solid. Earth* **1**, 5–24 (2010).
156. Wright, R. & Pilger, E. Radiant flux from Earth's subaerially erupting volcanoes. *Int. J. Remote Sens.* **29**, 6443–6466 (2008).
157. Hurwitz, S. Groundwater flow, heat transport, and water table position within volcanic edifices: implications for volcanic processes in the Cascade Range. *J. Geophys. Res.* **108**, 2557 (2003).
158. McCormack, F. S. et al. Fine-scale geothermal heat flow in Antarctica can increase simulated subglacial melt estimates. *Geophys. Res. Lett.* https://doi.org/10.1029/2022GL098539 (2022).
159. van der Veen, C. J., Leftwich, T., von Frese, R., Csatho, B. M. & Li, J. Subglacial topography and geothermal heat flux: Potential interactions with drainage of the Greenland ice sheet. *Geophys. Res. Lett.* https://doi.org/10.1029/2007GL030046 (2007).
160. Colgan, W. et al. Topographic correction of geothermal heat flux in Greenland and Antarctica. *J. Geophys. Res. Earth Surf.* **126**, e2020JF005598 (2021).
161. Colleoni, F. et al. Spatio-temporal variability of processes across Antarctic ice-bed–ocean interfaces. *Nat. Commun.* **9**, 2289 (2018).
162. DeConto, R. M. & Pollard, D. Contribution of Antarctica to past and future sea-level rise. *Nature* **531**, 591–597 (2016).
163. Fürst, J. J. et al. Assimilation of Antarctic velocity observations provides evidence for uncharted pinning points. *Cryosphere* **9**, 1427–1443 (2015).
164. Mengel, M. & Levermann, A. Ice plug prevents irreversible discharge from East Antarctica. *Nat. Clim. Change* **4**, 451–455 (2014).
165. Gulick, S. P. S. et al. Initiation and long-term instability of the East Antarctic Ice Sheet. *Nature* **552**, 225–229 (2017).
166. Robel, A. A., Seroussi, H. & Roe, G. H. Marine ice sheet instability amplifies and skews uncertainty in projections of future sea-level rise. *Proc. Natl Acad. Sci. USA* **116**, 14887–14892 (2019).
167. Van Liefferinge, B. et al. Promising oldest ice sites in East Antarctica based on thermodynamical modelling. *Cryosphere* **12**, 2773–2787 (2018).
168. Larour, E., Morlighem, M., Seroussi, H., Schiermeier, J. & Rignot, E. Ice flow sensitivity to geothermal heat flux of Pine Island Glacier, Antarctica. *J. Geophys. Res. Earth Surf.* https://doi.org/10.1029/2012JF002371 (2012).
169. Seroussi, H. et al. ISMIP6 Antarctica: a multi-model ensemble of the Antarctic ice sheet evolution over the 21st century. *Cryosphere* **14**, 3033–3070 (2020).
170. Pittard, M. L., Galton-Fenzi, B. K., Roberts, J. L. & Watson, C. S. Organization of ice flow by localized regions of elevated geothermal heat flux. *Geophys. Res. Lett.* **43**, 3342–3350 (2016).
171. Smith-Johnsen, S., Schlegel, N.-J., De Fleurian, B. & Nisancioglu, K. H. Sensitivity of the Northeast Greenland Ice Stream to geothermal heat. *J. Geophys. Res. Earth Surf.* **125**, e2019JF005252 (2020).
172. Lemieux, J. M., Sudicky, E. A., Peltier, W. R. & Tarasov, L. Simulating the impact of glaciations on continental groundwater flow systems: 2. Model application to the Wisconsinian glaciation over the Canadian landscape. *J. Geophys. Res. Earth Surf.* https://doi.org/10.1029/2007JF000929 (2008).
173. Elsworth, C. W., Schroeder, D. M. & Siegfried, M. R. Interpreting englacial layer deformation in the presence of complex ice flow history with synthetic radargrams. *Ann. Glaciol.* **61**, 206–213 (2020).
174. Guimarães, S. N. P., Vieira, F. P. & Hamza, V. M. Heat flow variations in the Antarctic Continent. *Int. J. Terr. Heat. Flow. Appl.* **3**, 1–10 (2020).
175. Purucker, M. *Antarctica Basal Heat Flux* (University of Montana, accessed 1 October 2012); http://websrv.cs.umt.edu/isis/index.php/Antarctica_Basal_Heat_Flux.
176. Morse, P. E., Reading, A. M. & Stål, T. Well-posed geoscientific visualization through interactive color mapping. *Front. Earth Sci.* **7**, 0–17 (2019).
177. Crameri, F. & Shephard, G. E. Scientific colour maps, https://doi.org/10.5281/zenodo.3596401 (Zenodo, 2019).
178. Dalziel, I. W. D. & Elliot, D. H. West Antarctica: problem child of Gondwanaland. *Tectonics* **1**, 3–19 (1982).
179. Cottrell, E. in *Volcanic Hazards, Risks and Disasters* (eds. Shroder, J. F. & Papale, P.) 1–16 (Elsevier, 2015).
180. Lemieux, J. M., Sudicky, E. A., Peltier, W. R. & Tarasov, L. Dynamics of groundwater recharge and seepage over the Canadian landscape during the Wisconsinian glaciation. *J. Geophys. Res. Earth Surf.* **113**, 1–18 (2008).

Acknowledgements

This work was supported in part by the Australian Research Council (ARC), through ARC DP190100418 (A.M.R., T.S.). Additional support was provided through ARC SRI Antarctica Gateway Partnership, SR140300001 (T.S.), ARC SRI Australian Centre for Excellence in Antarctic Science, SR200100008 (A.M.R., T.S., J.A.H.), ARC DP180104074 (J.A.H., D.H.) and ARC DECRA DE210101433 (F.S.M.). Further support was provided by the Deutsche Forschungsgemeinschaft in the framework of the priority programme 'Antarctic Research with comparative investigations in Arctic ice areas' SPP 1158 (grant no. EB 255/8-1, M.L., J.E.). The authors thank the many participants of the Scientific Committee on Antarctic Research, Scientific

Research Program on Solid Earth Response and influence on Cryosphere Evolution (SCAR, SERCE, to 2020) and its successor, Instabilities and Thresholds in Antarctica, subcommittee on Geothermal Heat Flow (SCAR, INSTANT, from 2021) for discussions that informed this Review.

Author contributions
A.M.R. conceived the review, drafted text and display items. T.S. drafted text and produced map and display items. All authors contributed to the text and refined the review.

Competing interests
The authors declare no competing interests.

Peer review information
Nature Reviews Earth & Environment thanks T. Jordan, K. Matsuoka and the other, anonymous, reviewer(s) for their contribution to the peer review of this work.

Publisher's note
Springer Nature remains neutral with regard to jurisdictional claims in published maps and institutional affiliations.

Supplementary information
The online version contains supplementary material available at https://doi.org/10.1038/s43017-022-00348-y.

RELATED LINKS
The Scientific Committee on Antarctic Research INSTANT initiative provides a further connection to legacy and current Antarctic GHF models at: https://www.scar-instant.org.